THE JOURNAL OF PHYSICAL CHEMISTRY B
A JOURNAL OF THE AMERICAN CHEMICAL SOCIETY

pubs.acs.org/JPCB Article

# Critical Beginnings: Selective Tuning of Solubility and Structural Accuracy of Newly Synthesized Proteins by the Hsp70 Chaperone System

Rayna M. Addabbo, Rachel B. Hutchinson, Heather J. Allaman, Matthew D. Dalphin, Miranda F. Mecha, Yue Liu, Alexios Staikos, and Silvia Cavagnero*

Cite This: https://doi.org/10.1021/acs.jpcb.2c08485 Read Online



**ABSTRACT:** Proteins are particularly prone to aggregation immediately after release from the ribosome, and it is therefore important to elucidate the role of chaperones during these key steps of protein life. The Hsp70 and trigger factor (TF) chaperone systems interact with nascent proteins during biogenesis and immediately post-translationally. It is unclear, however, whether these chaperones can prevent formation of soluble and insoluble aggregates. Here, we address this question by monitoring the solubility and structural accuracy of globin proteins biosynthesized in an *Escherichia coli* cell-free system containing different concentrations of the bacterial Hsp70 and TF chaperones. We find that Hsp70 concentrations required to grant solubility to newly synthesized proteins are extremely sensitive to client-protein sequence. Importantly, Hsp70 concentrations yielding soluble client proteins are insufficient to prevent formation of soluble aggregates. In fact, for some aggregation-prone protein variants, avoidance of soluble-aggregate formation demands Hsp70 concentrations that exceed cellular levels in *E. coli*. In all, our data highlight the prominent role of soluble aggregates upon nascent-protein release from the ribosome and show the limitations of the Hsp70 chaperone system in the case of highly aggregation-prone proteins. These results demonstrate the need to devise better strategies to prevent soluble-aggregate formation upon release from the ribosome.

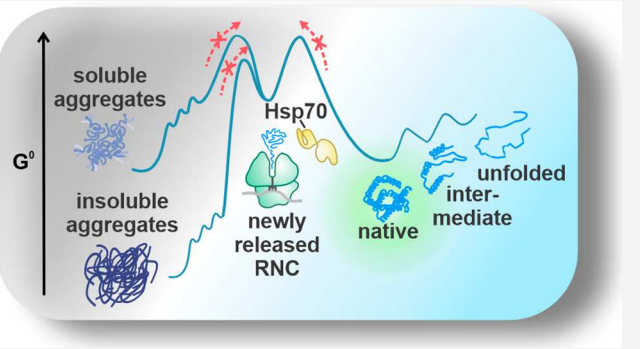




## INTRODUCTION

After biosynthesis, most *Escherichia coli* proteins and the model protein sperm whale apomyoglobin are kinetically trapped relative to a variety of aggregates (e.g., nonamyloid and amyloid[5]), in cell-like media under physiologically relevant conditions.[3,5b] However, transient non-native conformations generated immediately after nascent-protein release from the ribosome are not kinetically trapped relative to aggregates, presumably due to their high free energy and lower barriers to folding/aggregation. Indeed, these conformations experience a particularly high propensity to aggregate.[3,6] Recent studies showed that, upon release from the ribosome, kinetic channeling of nascent proteins toward either native or aggregated states is extremely sensitive to protein sequence. For instance, single-point mutations that perturb folding/unfolding/aggregation kinetic barriers upon release from the ribosome, but not native-state thermodynamic stability, cause proteins to be released from the ribosome as insoluble aggregates (Figure 1a).[3]

Molecular chaperones are known to facilitate protein folding, prevent aggregation, and perform a variety of additional critical cellular functions that enable cell survival and growth.[8] The Hsp70 system and trigger factor (TF) are the primary bacterial chaperones that act during the early co- and post-translational periods in protein life.[9] Client proteins bind Hsp70 according to their folding kinetics, equilibrium thermodynamic properties,[11] and aggregation propensity.[12] *E. coli* cells can tolerate the deletion of either Hsp70 (known as DnaK in *E. coli*) or TF. On the other hand, simultaneous deletion of both chaperones is lethal to cells at temperatures higher than 30 °C.[9a,13] While TF and Hsp70 have partially overlapping roles, Hsp70 enables bacterial cell viability across a wider temperature range than TF.[9a,13b]

Hsp70 and TF are not only important for wild-type cell viability but also serve as "buffers" against mutations in bacteria. For instance, overexpression of TF increases the in

Received: December 3, 2022
Revised: April 15, 2023





https://doi.org/10.1021/acs.jpcb.2c08485
J. Phys. Chem. B XXXX, XXX, XXX−XXX

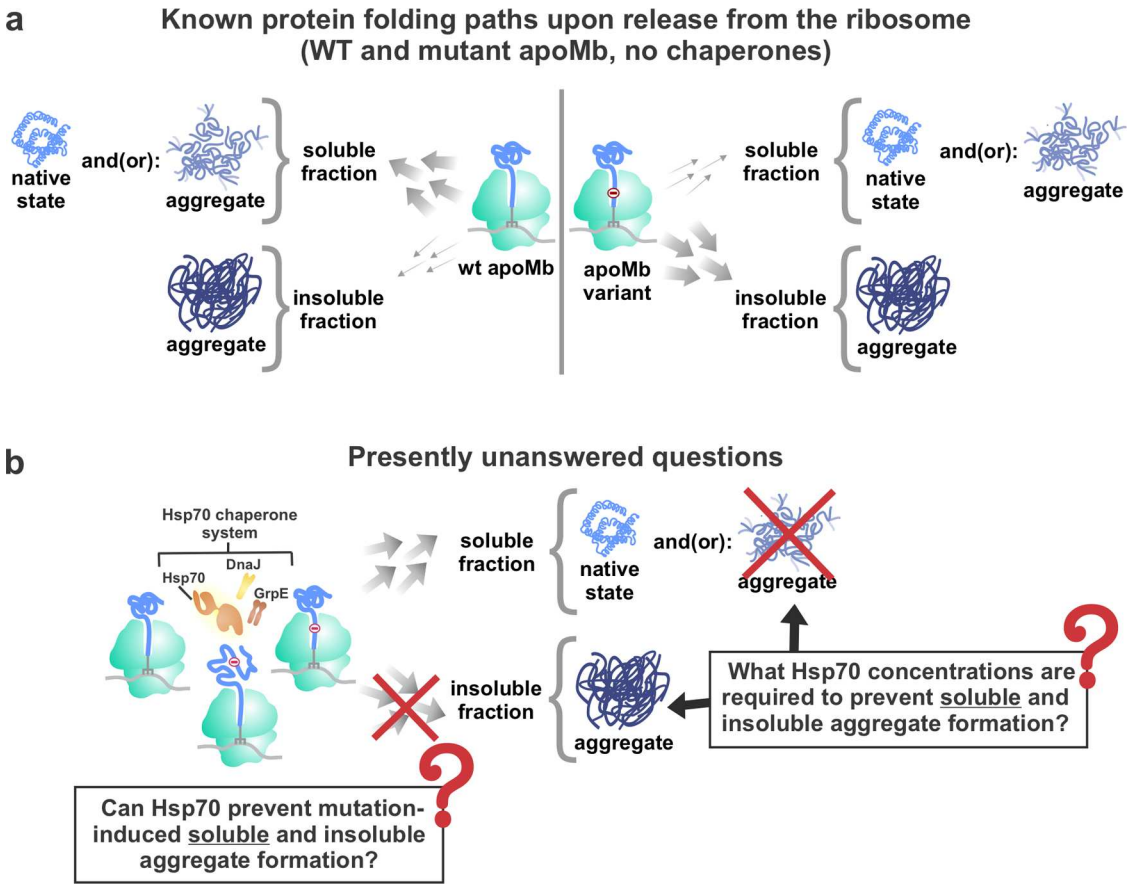


**Figure 1.** Key concepts and unanswered questions investigated in this study. (a) Upon protein biosynthesis at low concentrations ($0.3 \pm 0.2$ $\mu$M) in an *E. coli* cell-free system devoid of molecular chaperones, WT apoMb forms a soluble species. A single-point mutation (M131D) is known to disrupt the kinetic balance between protein folding and aggregation upon release from the ribosome (Addabbo et al. 2020) and causes apoMb to form an insoluble aggregate.[3] (b) Unanswered questions addressed in this work.

vivo activity and solubility of deleterious mutants of the *E. coli* controller of cell-death protein B (CcdB).[14] In addition, in evolving *E. coli* bacteria, overexpression of Hsp70 prevents cell-line extinction from the accumulation of random mutations across several proteins.[15] Further, *E. coli* proteins that interact more frequently with Hsp70[16] evolve faster than clients that interact less frequently with this chaperone.[15,17] The latter studies show that the Hsp70 and TF chaperones are capable of preventing harmful mutation-related phenotypes.

Despite the above knowledge, the types of mutations requiring chaperone assistance (e.g., surface vs core, stabilizing vs destabilizing) and the structural characteristics of ribosome-released client-protein variants (e.g., native states, soluble or insoluble aggregates) generated in the absence and presence of chaperones are not known.

Interestingly, one of the ways the Hsp70 and TF chaperones operate is by granting solubility to a variety of proteins, upon release from the ribosome. For instance, in the absence of any chaperone, 72% of *E. coli* proteins (excluding membrane proteins) are insoluble (<80% solubility) when synthesized on the ribosome via a cell-free transcription-translation system.[6] These studies were performed at 37 °C, and *E. coli* proteins were expressed at an average concentration of 33 $\mu$g/mL.[6] TF grants solubility (i.e., >50% increase in solubility) to only 2% of these aggregation-prone proteins.[18] On the other hand, Hsp70 renders 52% of these proteins soluble.[18] Further, in addition to increasing the solubility of *E. coli* homologous proteins,[18] Hsp70 and TF also perform a similar action on heterologous[19] proteins. It is imperative, however, to note that a protein's soluble status does not necessarily imply native conformation. For instance, soluble proteins, including members of the globin fold, sometimes populate soluble aggregates under physiologically relevant conditions.[3,20] Soluble aggregates are not bioactive and reduce the amount of functional gene product produced upon recombinant protein expression.[21] Further, in higher organisms including mammals, it is becoming clear that soluble aggregates contribute to a variety of deadly maladies.[22]

Despite the above progress, there is a crucial gap in knowledge about whether Hsp70 or TF can prevent the formation of soluble aggregates. In addition, it is not known what specific chaperone concentrations are required to prevent soluble and insoluble aggregate formation upon release from the ribosome (Figure 1b).

In this study, we focus on the well-biochemically characterized model protein apomyoglobin.[4,23] We explore the nature of its native state and its soluble/insoluble aggregates immediately upon release from the ribosome in the absence and presence of the Hsp70 and trigger factor (TF) chaperones.

Specifically, we employ apoMb as a benchmark to address two key unanswered questions, as schematically illustrated in Figure 1. Namely, (1) Can the Hsp70 chaperone system prevent the harm caused by single-point mutations that disrupt


https://doi.org/10.1021/acs.jpcb.2c08485
J. Phys. Chem. B XXXX, XXX, XXX−XXX

the apoMb nonpolar-core? and (2) what Hsp70 concentrations are needed to prevent soluble and insoluble aggregate formation of WT and mutant apoMb upon release from the ribosome? We employ a combination of site-specific fluorophore labeling, solubility assays, frequency-domain fluorescence lifetime and anisotropy decays, and multidimensional NMR. These synergistic approaches offer an excellent opportunity to identify both soluble and insoluble gene products and, importantly, to characterize the nature of the soluble fraction of newly synthesized proteins. We focus on the role of Hsp70 during the last stages of de novo protein biosynthesis. We evaluate two apoMb variants specifically designed to perturb co- and immediately post-translational conformational sampling. We show that physiologically relevant concentrations of Hsp70 prevent insoluble aggregate formation induced by single-point mutations. However, under nonstress conditions, higher than physiologically attainable Hsp70 concentrations[24] are required to prevent the generation of soluble aggregates. The wild-type protein also forms soluble aggregates with different characteristics, upon release from the ribosome. Therefore, different proteins have distinct Hsp70 chaperone requirements to prevent the formation of insoluble and soluble aggregates. Further, the *E. coli* Hsp70 chaperone system is incapable of reversing the deleterious effect of the M131D apoMb single-point mutation, which is known[3] to be responsible for incorrect kinetic channeling upon release from the ribosome. In all, this work demonstrates the crucial importance of controlling immediately post-translational events taking place upon release from the ribosome, and it shows that the Hsp70 chaperone system is capable of modulating this crucial step of protein life, but only to a limited extent.

## EXPERIMENTAL METHODS

**Generation of I28D and M131D apoMb Plasmids.** In order to generate plasmids containing the I28D and M131D point mutations, the Quikchange II Site-Directed Mutagenesis Kit was used. Single-codon mutations were inserted starting from the pET-Blue1 plasmid harboring the WT sperm whale apoMb gene.

**Cell-Free Transcription-Translation.** Ribosome-released proteins were produced as previously described.[25] In summary, a pET-Blue1 plasmid (24−50 $\mu$g/mL) containing genes encoding WT sperm whale apoMb, or I28D apoMb[26] was employed in either a WT or Δtig (lacking endogenous TF) A19 *E.coli* transcription-translation system prepared in-house.[4] The endogenous concentration of Hsp70, DnaJ, and GrpE in the cell-free systems are approximately 0.5, 0.04, and 0.05 $\mu$M, respectively. The endogenous concentration of TF in the WT cell-free system is 0.2 $\mu$M. Cotranslational site-specific N-terminal labeling of expressed apoMb was achieved by the addition of in-house prepared BODIPY-FL-Met-tRNA$^{fMet}$.[25] When applicable, the KLR-70 Hsp70 inhibitor was added to a final concentration of 400 $\mu$M to produce apoMb in the absence of Hsp70. All cell-free transcription-translation reactions were carried out at 37 °C for 20 min. Full-length ribosome-released WT apoMb was produced in the presence of added purified Hsp70, DnaJ, and GrpE. The final concentrations of Hsp70 were approximately 21 or 75 $\mu$M. DnaJ was present at final concentrations of 0.04−12 $\mu$M. GrpE was present at approximately 19 $\mu$M.

**Determination of apoMb Concentrations in Cell-Free Systems.** The concentration of apoMb produced in cell-free systems according to identical procedures to those employed here was previously determined to be 300 nM via Western blotting.[3] The standard error in total apoMb fluorescence intensity (soluble plus insoluble fractions) in the SDS-PAGE gels for solubility experiments (Figure 4) was used to calculate uncertainties in apoMb concentration. Gel band intensities were quantified with ImageJ.[27] Standard error and percent error for apoMb total fluorescence intensities are listed in Supporting Table S1. The average percent error for all three species was 49%. Therefore, the uncertainty for the apoMb concentration was calculated to be 0.15 $\mu$M, and the apoMb concentration is reported as 0.3 ± 0.2 $\mu$M. This uncertainty was propagated to determine the uncertainty in chaperone-to-apoMb-protein ratios listed in Figures 4 and 8.

**Yields of WT and Variant apoMb Cell-Free Production.** The yields of total protein production upon transcription-translation in the in-house *E. coli* cell-free system employed here were qualitatively estimated by inspection of low-pH gels.[28] As shown in Supporting Figure S1b, WT, I28D, and M131D apoMb were produced with comparable yields under the same experimental conditions. Given that protein production velocity is likely dominated by the rate-determining translation-elongation rates (once transcription lag times are factored out), this observation supports the idea that production of the variants studied in this work does not involve changes in translation rates, relative to the parent WT protein.

**Overexpression and Purification of TF and Hsp70 Chaperones.** The Hsp70 chaperone was prepared according to known procedures.[29] Hsp70 concentration was determined by electronic absorption spectrophotometry, using extinction coefficient $\varepsilon$ = 15,930 $M^{-1}$ $cm^{-1}$ at 280 nm, estimated according to known procedures.[30] The TF chaperone was overexpressed and purified as described,[31] and its concentration was determined by electronic absorption spectrophotometry using extinction coefficient $\varepsilon$ = 17,420 $M^{-1}$ $cm^{-1}$ at 280 nm, which was estimated according to Gill and von Hippel.[30]

**SDS-PAGE Gel Solubility Assays.** Cell-free expressed apoMb with an N-terminal BODIPY-FL fluorophore was centrifuged at 15,800 rcf and 4 °C for 20 min. The resulting pellet was separated from the supernatant and resuspended in resuspension buffer (10 mM Tris−Cl pH 7.0, 10 mM $Mg(OAc)_2$, 60 mM ammonium chloride, and 0.5 mM EDTA). The resulting supernatant and pellet fractions were then run on a low-pH SDS-PAGE gel as described previously.[28] The fluorophore-labeled apoMb in each fraction was subsequently visualized using an FLA 9500 Typhoon Gel Imager with a 488 nm excitation laser and 500−550 nm band-pass emission filter (BPB1). Molecular weight markers were visualized with a 635 nm excitation laser and a 675 nm long-pass filter (LPR). The apoMb band intensities in both fractions were then analyzed using the ImageJ software package.[27] The percent of soluble protein in each sample was then calculated by the following expression, where $I_{soluble}$ and $I_{insoluble}$ are the fluorescent band intensities of the soluble and insoluble fractions, respectively

$$\%\ \text{solubility} = \frac{I_{soluble}}{I_{soluble} + I_{insoluble}} \times 100 \quad (1)$$

When calculating the percent solubility of apoMb RNCs, the soluble and insoluble band intensities were calculated as the


https://doi.org/10.1021/acs.jpcb.2c08485
J. Phys. Chem. B XXXX, XXX, XXX−XXX

difference in intensity between samples treated without and with puromycin.

**Post-Translational Kinetic Trapping of Soluble and Insoluble States of Newly Synthesized Protein.** Experiments shown in Figure 5 were performed as follows. Ribosome-released M131D and I28D apoMb were generated as described above in the absence of chaperones, in a Δ*tig* S30 system, in the presence of an Hsp70 chaperone inhibitor[1] (150 μM). The process was quenched by placement on ice. Soluble and insoluble protein fractions were separated by centrifugation at 15,800 rcf at 4 °C for 20 min. The pellet was resuspended, either in the same volume as the original reaction or diluted 1:10, in a cell-free transcription-translation solution, either with or without ATP, containing all components except for T7 RNA polymerase, BODIPY-FL-Met-tRNA$^{fMet}$, and plasmid DNA, to prevent further protein production. Additionally, puromycin (1 mM, in 10 mM Tris, 11 mM $Mg(OAc)_2$, 60 mM $NH_4Cl$, 0.5 mM EDTA at pH 7) was added to both the supernatant and resuspended pellet to further ensure that no additional protein synthesis would occur. Supernatant and resuspended pellet were incubated at 37 °C for ca. 14 h, and then placed on ice. The solutions were then centrifuged at 15,800 rcf at 4 °C for 20 min. Pellets were resuspended in loading buffer (83 mM TrisBase, 3.8 M glycerol, 116 mM SDS, pH 5.7). All samples were subject to low-pH SDS-PAGE, and gel band intensities were quantified with ImageJ. Intensities from samples on different gels were normalized using the tRNA intensity, where the tRNA concentration is about 11.67 μM, first diluted 0.1:25 in RNase-free water and then 1:11 in loading buffer.

**Fluorescence Lifetime and Anisotropy Decay.** An ISS Chronos spectrophotometer was used to collect lifetime and depolarization data as previously reported.[32] A 477 nm laser diode was used to excite fluorescently labeled samples. A 480 nm band-pass excitation filter and a 495 nm long-pass emission filter (HHQ495lp, Chroma) were used. The instrument has calcite prism polarizers. For both lifetime and depolarization experiments, samples were excited with the excitation polarizer in the vertical position. For lifetime experiments, the emission polarizer was set to the magic angle, 54.7°. The spectrophotometer was temperature-regulated using a water bath set to 25 °C. Samples were temperature preequilibrated in the instrument before data collection for ≥30min. Fluorescence depolarization experiments were corrected using an independent G experiment, performed for each experimental day, as described by Knight et al.[32]

Lifetime and depolarization experiments were fit in the Globals Software Suite (LFD). $X^2$ was calculated for all fits, assuming an instrumental error in the modulation of 0.004 and an instrumental error in the phase of 0.2°.[33] All lifetime data were fit to three exponential decay expressions. The first two discrete components were determined by the fit and are the fluorescence lifetimes of the labeled samples. A third fictitious 1 ps lifetime was fixed in the fit, to account for an extremely small amount of scattering in the sample. Lifetime phasors[34] were calculated at 23.08 MHz for full-length WT apoMb produced in the cell-free system without stalling (Figure 6b). The following expressions were used

$$G = M \cos \phi \tag{2}$$

$$S = M \sin \phi \tag{3}$$

where $\phi$ is the phase shift between the excitation and emission light intensity profile and $M$ is the frequency-domain modulation, which is defined as[35]

$$M = \frac{AC_{EM}/DC_{EM}}{AC_{EX}/DC_{EX}} \tag{4}$$

where AC is the amplitude of the light intensity wave and DC is the average intensity. The EM and EX subscripts refer to the emission and excitation light, respectively. Fluorescence depolarization experiments on WT apoMb and M131D apoMb were fit to three-component exponential decay expressions, which resulted in at least 2-fold reduction in the calculated $X^2$ of the fit, relative to the $X^2$ of the two-component exponential decay fits. Ribosome-released proteins were fit to either a two-component or three-component exponential decay fit. Three-component exponential decay fits were only used if they resulted in a 2-fold or greater reduction in the calculated $X^2$ relative to the two-component exponential decay fits. Order parameters and cone semiangles were calculated according to Ellis et al.[36]

**Lifetime Phasor Analysis to Estimate the Mole Fraction of Soluble Aggregate Produced in the Absence of DnaK.** This section describes the method to calculate the percent soluble aggregate reported in Figure 8. NMR experiments were only able to detect 23.5% of apoMb protein made in the absence of chaperones. Therefore, we estimated that this sample, which contained 59.8 μM protein contained 76.5% soluble aggregates. The samples used for fluorescence lifetime and anisotropy experiments contained 0.3 ± 0.2 μM apoMb protein. Since the fluorescence samples lacking chaperones contained a lower concentration than the samples used for NMR, we concluded that these samples would have at most 76% soluble aggregates. The fluorescence lifetime phasor of WT apoMb shifts along a straight line depending on the relative concentration of soluble aggregate and native protein (Figure 8c).[3] The lifetime phasor for purified apoMb was generated from fluorescence data of E41C apoMb that was overexpressed in *E. coli*, and labeled with BODIPY-FL at the mutated cysteine position via an ester bond. The purified and labeled protein was refolded in a solution containing unlabeled ribosome-bound nascent chains.[37] The concentration of ribosomes in this experiment was similar to the concentration of ribosomes in the fluorescence experiments described in the main text of this work. In this work, we reanalyzed the previously published fluorescence data to determine the phasor plot point for the pure native state with no soluble aggregates. The phasors for all samples were calculated from the fluorescence lifetime data using eqs 2 and 3. $G$ is plotted on the $x$-axis and $S$ is plotted on the $y$-axis of the phasor plot. For this work, all phasors were calculated using the $M$ and $\phi$ values at the 23 MHz modulation frequency. The universal circle is defined by

$$\left(G - \frac{1}{2}\right)^2 + S^2 = \frac{1}{4} \tag{5}$$

We then used the experimental phasors to predict the phasor for a sample that contained 100% soluble aggregates. The predicted phasor was calculated using eqs 6−8.

$$G_{mix} = f_{SA} G_{SA} + f_N G_N \tag{6}$$

$$S_{mix} = f_{SA} S_{SA} + f_N S_N \tag{7}$$



https://doi.org/10.1021/acs.jpcb.2c08485
J. Phys. Chem. B XXXX, XXX, XXX−XXX

$$f_{SA} + f_N = 1 \quad (8)$$

where $G_{mix}$ and $S_{mix}$ are the experimental phasor coordinates for apoMb produced in the absence of Hsp70; $f_{SA}$ and $f_N$ are the fractions of the total fluorescence intensity of the mixture due to the soluble aggregate and native state, respectively; and $G_{SA}$, $S_{SA}$, $G_N$, and $S_N$ are the phasor coordinates for the pure soluble aggregate and native state. We assumed that the purified protein sample contained no soluble aggregates, and we assumed that the sample made without chaperones had ≤76.5% soluble aggregates. We also assumed that all samples contained only two species: the native state and soluble aggregates. After calculating the predicted phasor for pure soluble aggregates, we used these values to estimate the percent soluble aggregates for the other chaperone conditions. We calculated the percent soluble aggregate for each condition by using the experimental phasor coordinates for $G_{mix}$ and $S_{mix}$, the predicted phasor coordinates for the soluble aggregates for $G_{SA}$ and $S_{SA}$, and the experimental phasor coordinates for purified apoMb for $G_N$ and $S_N$. From these equations, we solved for $f_{SA}$ and $f_N$.

The maximum percent of soluble aggregates for each chaperone concentration was used to plot the percent soluble aggregates vs the concentration of Hsp70. The linear fit for these plots was used to estimate the amount of Hsp70 required to eliminate soluble aggregates in WT and Δtig S30.

**In Vivo apoMb Expression and Purification.** Large-scale overexpression and purification of WT, M131D, and I28D apoMb were carried out as described.[3] A pET-Blue1 plasmid containing the I28D mutation was used to generate this variant. Purified proteins were identified with MALDI mass spectrometry. The experimental molecular weights matched the expected molecular weights for all three species (WT apoMb: 17,331 amu; M131D apoMb: 17,315 amu; I28D: 17,333 amu).

**NMR Sample Preparation.** Selectively labeled apoMb containing $^{15}$N A, E, L, K, V, and $^{15}$N−$^{13}$C W analyzed in NMR experiments was generated via cell-free expression and the same dialysis procedure described by Addabbo et al.[3] The only difference in the dialysis procedure for this work was that apoMb was generated with WT S30 containing endogenous chaperone concentrations (0.5 μM Hsp70, 0.04 μM DnaJ, 0.05 μM GrpE, and 0.2 μM TF). Prior to NMR analysis, 40 μL of $D_2O$ was added to 360 μL of sample the cell-free mixture and loaded onto a 5-mm-diameter Shigemi tube (Wilmad, BMS-005B). A negative control sample was prepared as above, except that no T7 RNA polymerase was added, to prevent gene expression. SDS-PAGE gel analysis was used to determine the apoMb concentration of NMR samples. A calibration curve was generated from the gel intensity of cell-free reactions containing different known concentrations of apoMb. The calibration curve was used to calculate the apoMb sample concentration used for NMR experiments ([total apoMb]). Gels were stained with Coomassie blue and imaged on a Typhoon FLA 9500 (GE Healthcare) upon excitation with a 532 nm laser in the presence of a 575 nm long-pass filter. apoMb gel band intensities were quantified with the ImageJ software.[27]

**NMR Data Collection, Processing, and Volume Analysis.** NMR spectra were collected and processed as described.[3] Data in Figure 8a,b were collected with 740 and 700 scans per row, respectively. Volume analysis of NMR resonances was carried out to estimate the fraction of spectroscopically undetectable apoMb protein due to extremely slow tumbling[38] and slow translational diffusion,[39] as described.[3] Briefly, the 2D NMR volume of the $^1$H−$^{15}$N resonance corresponding to the free-Trp indole ($Vol_{Trp}$) was measured with the NMRViewJ software for a sample containing 800 μM of free-Trp. The volumes of the following clearly resolved apoMb resonances were measured ($Vol_{res}$): V17, A19, A22, A57, K62, K78, or A130. Then, the apoMb concentration was calculated with eq 9[3]

$$\frac{Conc_{Trp}}{Vol_{Trp}} \times Vol_{res} = Conc_{res} \quad (9)$$

The seven separate $Conc_{res}$ values were averaged to calculate the concentration of native apoMb detected by NMR ($[Native]_{NMR}$). The percent native protein was calculated with eq 10

$$\% \text{ native} = \frac{[Native]_{NMR}}{[\text{total apoMb}]} \times 100\% \quad (10)$$

where [total apoMb] is the total apoMb protein concentration determined by SDS-PAGE gel analysis with a calibration curve generated with apoMb standards of known concentration. Signal-to-noise ratios (S/N), defined as the ratios of the intensity of the resonance of interest to the r.m.s. noise amplitude,[40] are reported in Supporting Table S2. Percent of native state and total NMR data collection times are shown in Table 3.

**Characterization of WT apoMb and apoMb Variants.** The secondary structure of WT apoMb and apoMb variants was assessed with circular dichroism, as described previously.[3] The thermodynamic stability of the WT and variant apoMb proteins was assessed by Trp fluorescence upon denaturation with urea, as described in Addabbo et al.[3] The Hsp70 binding sites for the proteins were identified with the algorithm developed by Rüdiger et al.[41]

## RESULTS AND DISCUSSION

**Design Criteria.** Sperm whale apomyoglobin (apoMb), the model protein selected for these studies, has a number of desirable properties, as briefly detailed below. First, apoMb belongs to the ubiquitous globin fold,[42] which is also highly represented in bacteria,[42c] and its three-dimensional structure has been thoroughly characterized.[43] Second, the size and hydrophobicity/charge pattern of apoMb[44] are typical of those encountered across the *E. coli* proteome.[45] It is worth noting that the codon usage of our wild-type and mutant apoMb-encoding plasmids have been optimized for *E. coli*.[46] Third, apoMb is a well-biochemically characterized protein[23a,f,47] that has been an important model system for detailed experimental investigations on protein folding paths upon refolding into buffered solution[23b,c,g,48] and within the cellular environment.[3,4,25,26,36,44,49] Fourth, apoMb is a quintessential example of the many proteins that are unable to reach their native state at 100% level upon refolding from denaturant.[50] Indeed, purified chemically denatured wild-type apoMb forms some soluble aggregates upon refolding into buffer.[51] Further, upon biosynthesis in an *E. coli* transcription-translation cell-free system (at ca. 0.3 μM expression level) lacking chaperones, wild-type apoMb gives rise to large slowly tumbling species that were recently attributed to soluble aggregates.[3] This adduct may include homo- or hetero-aggregates, associated via either specific or nonspecific interactions.[3] On the other hand,


https://doi.org/10.1021/acs.jpcb.2c08485
J. Phys. Chem. B XXXX, XXX, XXX−XXX

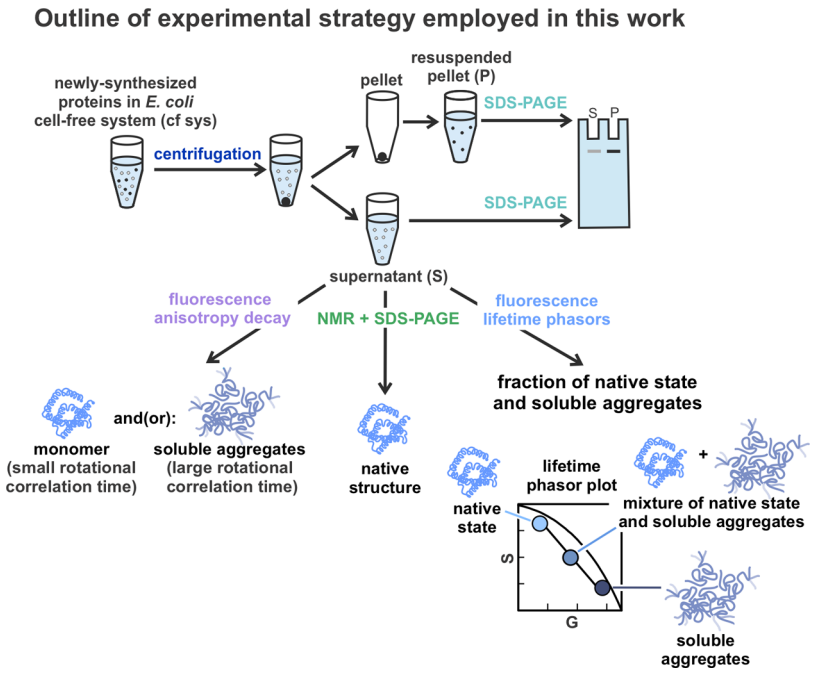


**Figure 2.** Overview of techniques employed in this work. Solubility assays were used to separate insoluble and soluble fractions. NMR spectroscopy in combination with SDS-PAGE was employed to identify the percent of newly synthesized protein in its native state. Fluorescence anisotropy decays revealed the size of local and global tumbling units and the amplitude of local motions. In addition, fluorescence emission frequency shifts showed changes in environment polarity and fluorescence lifetimes identified variations in local environment. Fluorescence lifetime phasors served to quantify fractions of monomeric protein and(or) soluble aggregates. All measurements targeted the characterization of newly synthesized proteins within the cell-free-system environment.

the nature of the apoMb-soluble fraction and the role of the Hsp70 chaperone upon transcription-translation are still very poorly understood. Further, at very high expression levels upon recombinant overexpression, apoMb gives rise to insoluble aggregates, a.k.a. inclusion bodies.[26,52] Fifth, apoMb has several Hsp70 binding sites,[53] and it interacts with this chaperone transiently upon refolding from denaturant, but not in its fully folded state, in buffered solution.[54] The effect of Hsp70 in a cell-like environment is not clear, especially in regard to the prevention of soluble-aggregate formation. In summary, apoMb and its variants are excellent model proteins to explore the effect of the Hsp70 chaperone system on protein solubility and structural accuracy upon nascent-protein release from the ribosome.

Newly synthesized proteins are generated via an in-house-produced *E. coli* cell-free system[55] and are *in situ* site-specifically labeled with the BODIPY- FL fluorophore at the N terminus.[25] This selective labeling procedure enables specific detection of the desired newly synthesized proteins by fluoroimaging and fluorescence lifetimes and anisotropies (see below). The high sensitivity of fluorescence enables detection of a wide range of chaperone-to-client-protein ratios (>100-fold).

As schematically illustrated in Figure 2, we discriminate soluble from insoluble fractions of fluorophore-labeled newly synthesized apoMb by SDS-PAGE. Then, we proceed with further analysis of the composition and dynamic characteristics of the soluble fraction. Namely, we discriminate native states from very slow-tumbling species in solution and quantify their relative amounts via a combination of 2D NMR and SDS-PAGE in the presence of apoMb calibrants of known concentration. To assess environmental differences, particle size, and amplitude of local motions, we employ frequency-domain fluorescence spectroscopy and measure fluorescence lifetimes and anisotropy decays.

**Design and Biophysical Characterization of I28D and M131D apoMb Variants.** We designed, produced, and analyzed single-point apoMb variants with the goal of probing the role of co- vs post-translational events in protein folding and aggregation. Toward this end, we replaced single nonpolar residues located in the central region of the native-protein hydrophobic core[43] with aspartic acid. This type of mutation is known to be well tolerated by proteins[56] and to slow down the acquisition of the native state.[57] We designed the I28D and M131D variants with the following criteria in mind. When native apoMb has been fully synthesized but before it is released from the ribosome, the I28D mutation site must reside outside of the ribosomal exit tunnel, within the ribosome-bound nascent chain (RNC). This concept is pictorially illustrated in Figure 3a. On the other hand, the M131D mutation must reside inside the ribosomal exit tunnel, as shown in Figure 3a for the M131D apoMb variant. The above geometrical arguments are supported by our knowledge of the ribosome structure,[58] including the conformational features of the ribosomal exit tunnel[59] and by the known number (30−35) of nascent-chain residues buried inside the tunnel within known proteomes.[58a,60] In addition, given the size of the known compact N-terminal domain of ribosome-bound nascent apoMb (ca. 60−80 N-terminal residues[25,44]), the negatively charged aspartic acid of the I28D variant must reside within the compact N-terminal region outside of the ribosomal tunnel core.[31,36] Therefore, the I28D apoMb variant may perturb conformational sampling either co- or post-translationally, given that the perturbed compact domain can exert its effect during biosynthesis or after nascent-protein release from the ribosome.


https://doi.org/10.1021/acs.jpcb.2c08485
J. Phys. Chem. B XXXX, XXX, XXX−XXX

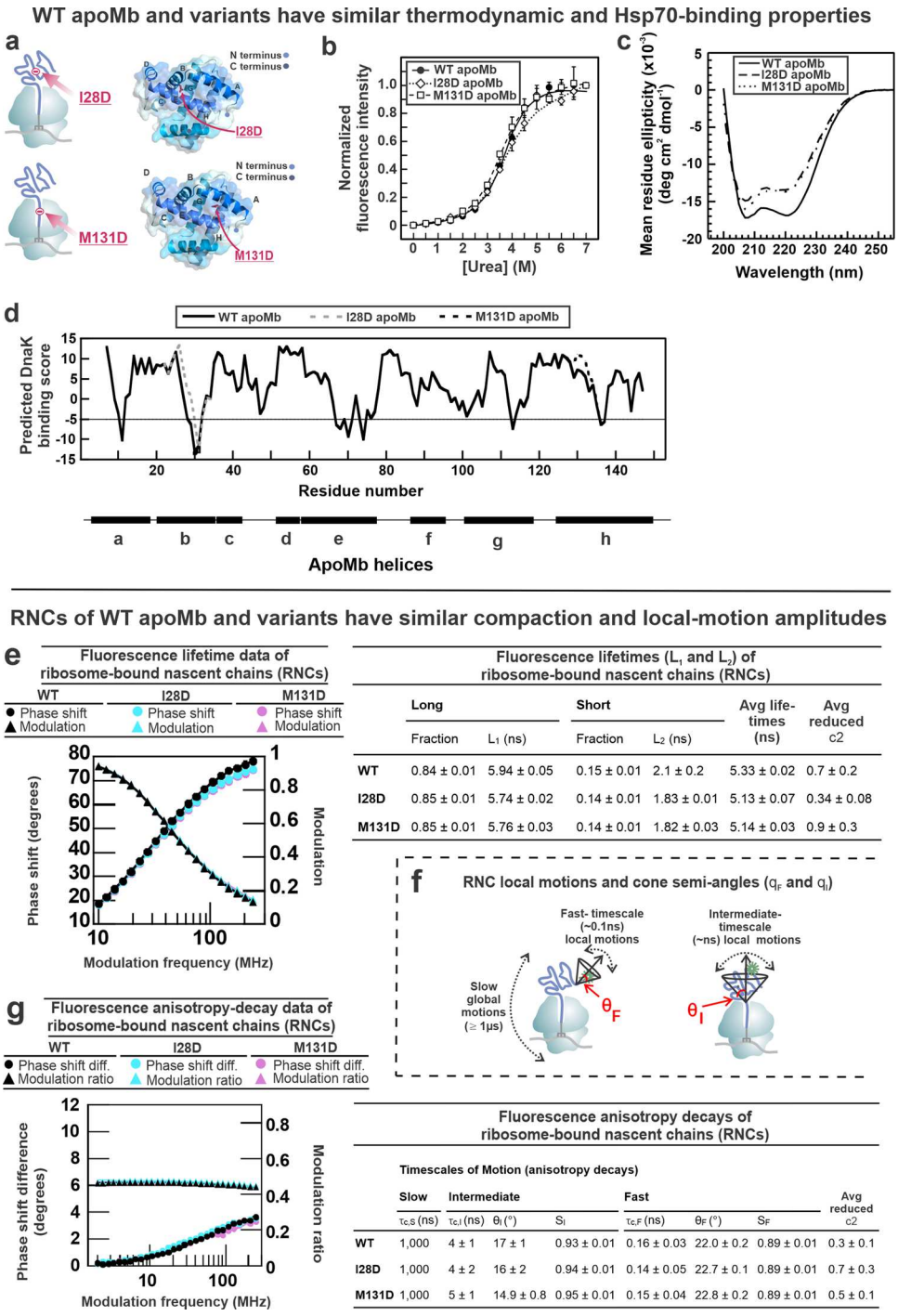


**Figure 3.** Biophysical characterization of I28D and M131D apoMb variants. (a) Mapping of mutations sites across full-length apoMb RNCs (left) and folded protein (right, PDB code 1MBC[2]). (b) Representative Trp fluorescence urea titration curves ($n$ = 3) of newly synthesized and purified apoMb and variants. (c) Far-UV circular dichroism spectra of purified WT apoMb and variants ($n$ = 3). (d) Probability scores for Hsp70 binding to WT apoMb and variants assessed via the algorithm by Rüdiger et al. Negative values denote greater binding probability. Representative fluorescence (e) lifetime and (f, g) anisotropy decays of full-length WT and variant apoMb RNCs, and tables including fitted parameters ($n$ = 2−3, avg ±SE). The symbols $\theta_I$ and $\theta_F$ denote cone semiangles for intermediate- and fast-timescale local motions, respectively. Data for WT and M131D data in (b), (c), (e), and (g) are reproduced with permission from ref 3. Copyright 2020 American Chemical Society.

In contrast, the M131D apoMb mutation is located only 23 residues away from the C-terminus of the full-length RNC, i.e., close to the peptidyl transferase center (PTC) and within the core of the ribosomal exit tunnel.[60] The negative charge of aspartic acid 131 is deeply buried inside the exit tunnel core of the respective RNC while the known compact partially folded N-terminal domain[25,36] lies within the N-terminal region of the chain. Therefore, the effect of the M131D mutation can primarily be sensed during conformational sampling events that enable contacts between the N-terminal portion of the chain and the D131 residue. These events necessarily take place after nascent-protein departure from the ribosomal tunnel, i.e., post-translationally. In summary, the M131D


https://doi.org/10.1021/acs.jpcb.2c08485
J. Phys. Chem. B XXXX, XXX, XXX−XXX

variant is mainly expected to perturb post-translational conformational sampling events.

Figure 3b–d shows the experimental biophysical characterization of the I28D and M131D apoMb variants. Urea titrations performed on the purified proteins (Figure 3b) indicate that the unfolding free energies ($\Delta G°$) and m-values[61] of WT, I28D, and M131D apoMb are all the same within error (Table 1). Therefore, these mutations do not influence the overall protein stability. Far-UV circular dichroism (CD) spectra show that the I28D and M131D variants experience a small loss in $\alpha$-helical content in their native states, relative to WT apoMb (Figure 3c). This decrease in helicity is likely due to small structural rearrangements that are known to occur when charged residues are introduced within protein interior locations.[62] Importantly, Figure 3d also shows that the I28D and M131D mutations are predicted to carry similar Hsp70 binding sites to the WT protein.[41,53] Hsp70 binding sites were predicted according to the algorithm by Rüdiger et al.,[41] where scores <5 denote high Hsp70 binding site probability.

**Table 1. Standard-State Unfolding Free Energies ($\Delta G°$) and *m*-Values of WT apoMb and Its Variants Determined via Urea Titrations**[a]

| protein | $\Delta G°$ (kcal mol$^{-1}$) | m-value (kcal mol$^{-1}$ M$^{-1}$) |
|---|---|---|
| WT apoMb | 5 ± 1 | −1.2 ± 0.3 |
| I28D apoMb | 4.6 ± 0.2 | −1.24 ± 0.01 |
| M131D apoMb | 4 ± 1 | −1.2 ± 0.3 |

[a]Reported values represent avg ± SE for $n$ = 3.

We also tested the overall conformational characteristics and local dynamics of full-length WT and mutant apoMb RNCs. The data are shown in Figure 3d,f. First, RNCs were analyzed by monitoring fluorescence lifetimes in the frequency domain,[33,35,63] after site-specifically labeling the nascent-protein N terminus with the BODIPY-FL fluorophore as described.[25] As shown in Figure 3d, the overall environment surrounding the N-terminus of WT, I28D, and M131D RNCs is very similar though not identical, given that the BODIPY-FL fluorescence lifetimes of the two variant apoMb RNCs are slightly smaller than the corresponding values of WT apoMb RNCs. Fluorescence lifetimes are extremely sensitive reporters of electrostatic and nonpolar chemical environment.[64] The moderately different fluorescence lifetimes show that even single-point nascent-chain mutations can lead to small variations in environment. This result is especially intriguing in the case of the apoMb M131D variant, whose mutation site is buried inside the ribosomal exit tunnel. Yet, the M131D nonpolar-to-charged mutation can be sensed close to the ribosomal surface, perhaps via some small long-range electrostatic effects. Nonetheless, this lifetime dependence is weak, and the observed changes are much tinier than other lifetime effects detected for different variant RNCs.[32] Next, we compared the compaction and local motions of WT and variant RNCs via frequency-domain fluorescence anisotropy decays.[35] As shown in Figure 3f, both WT and variant apoMb RNCs have intermediate-timescale local motions, which report on the compaction of the N-terminal ribosome-bound nascent-chain region, ranging from 4 to 6 ns. The corresponding size of these compact domains, based on reference WT RNC measurements,[44] varies between 57 and 83 residues depending on RNC shape. As shown in Figure 3f, the cone semiangles ($\theta_I$) describing the amplitude of the N-terminal motions are the same within error for WT and variant RNCs, and range between 14 and 16 degrees. The implications of the fluorescence lifetime and anisotropy data for the I28D apoMb variant are interesting. While these results indicate that apoMb RNCs can accommodate an aspartic acid at position 28 without resolvable disruption to the compact state, we cannot rule out more subtle disruptions to cotranslational folding that are not resolvable by fluorescence anisotropy decay analysis. Therefore, the nascent chains of all three species are equally compact, and the amplitudes of the local motions of the compact domains of all species are also indistinguishable and small.

Finally, we monitored the solubility of WT and variant RNCs in the absence and presence of molecular chaperones. The data, reported in Supporting Figure S1, show that all RNCs of the three types (i.e., WT, I28D, and M131D RNCs) are qualitatively similar, i.e., partially insoluble in the absence of chaperones and fully soluble in the presence of Hsp70 and TF chaperones. Some of these results were already reported earlier for WT and M131D apoMb.[3] These data confirm the earlier finding that the ribosome is an RNC-solubilizing agent,[3] possibly due to its high net charge and charge-segregation properties,[65] and that the TF and Hsp70 chaperones further enhance cotranslational RNC solubility.[3]

In all, our data show that the designed variants do not cause significant changes in native structure, thermodynamic stability, and Hsp70 binding site distribution and affinity, relative to WT apoMb. Further, the compaction, size, local dynamics, and solubility of WT and variant ribosome-bound nascent chains (RNCs) are also very similar or identical. Therefore, our results, discussed in the next sessions, can be interpreted upon ruling out the contributions of each of the above parameters.

**Hsp70 and TF Chaperones Prevent Insoluble-Aggregate Formation by Disruptive Point Mutations, upon Release from the Ribosome.** WT apoMb and the two variants described in the previous sections were employed to probe the effect of the Hsp70 and TF molecular chaperones on nascent-protein release from the ribosome. In this part of our study, we focused on the newly synthesized protein solubility. WT apoMb and its variants were biosynthesized in an *E. coli* cell-free transcription-translation system lacking or including increasing amounts of the Hsp70 and TF molecular chaperones, up to physiologically relevant concentrations of ca. 50 $\mu$M.[24] The data, displayed in Figure 4, show that WT apoMb attains greater than 90% solubility even in the absence of chaperones. Thus, WT apoMb does not need molecular chaperones for solubility. Indeed, as previously demonstrated,[3] the ribosome alone is fully responsible for the generation of a soluble WT apoMb gene product in the absence of any chaperones,[3] at total expressed-protein concentration of 0.3 $\mu$M.

In contrast, as shown in Figure 4a, the I28D and M131D apoMb variants are partially insoluble when biosynthesized in the absence of chaperones. Next, we analyzed the effect of adding increasing amounts of chaperones to independently biosynthesized WT and apoMb variants. We directed our initial focus on the Hsp70 chaperone system, which comprises *E. coli* Hsp70 or DnaK (K), and the cochaperones DnaJ (J) and GrpE (E). We found that an increase in the concentration of the Hsp70 system, in the absence of TF, increases the solubility of the I28D and M131D apoMb mutants (Figure 4a). Interestingly, only 6.5 $\mu$M Hsp70 is required to increase


https://doi.org/10.1021/acs.jpcb.2c08485
J. Phys. Chem. B XXXX, XXX, XXX−XXX

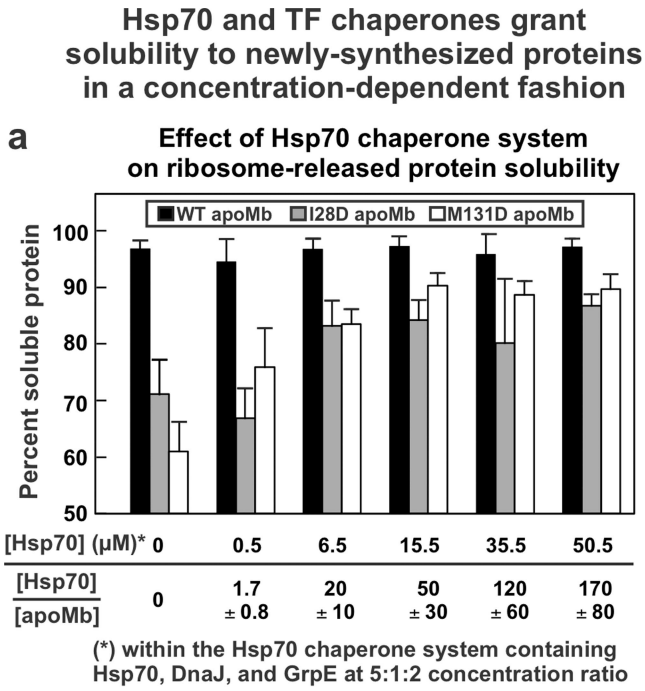


**Figure 4.** Hsp70 chaperone system and TF grant solubility to I28D and M131D apoMb variants. (a) Solubility of WT, I28D, and M131D apoMb generated at increasing Hsp70 concentrations in a TF-depleted Δtig *E. coli* cell-free system (cfs). DnaJ and GrpE were added so that relative K/J/E ratios were 5:1:2, except for the 0.5 $\mu$M Hsp70 data, where DnaJ and GrpE were 0.04 and 0.05 $\mu$M, respectively. apoMb concentration was 0.3 ± 0.2 $\mu$M. (b) Solubility of WT, I28D, and M131D apoMb produced at increasing TF concentrations in the presence of an Hsp70 inhibitor in a Δtig *E. coli* cfs. Statistical p values for data in both panels are in SI Tables S3 and S4.

the solubility of both mutants to a >80% solubility level. Physiologically relevant concentrations of Hsp70 (50 $\mu$M) restore the solubility of both mutants to near wild-type levels (87−90% soluble).

Then, we explored the effect of the TF chaperone on the solubility of newly synthesized WT apoMb and its variants. We found that TF increases the solubility of both variants to a similar extent as Hsp70 (Figure 4b). This result is consistent with the known overlapping roles of the two chaperones.[9a,13b]

In summary, the restored solubility of both variants shows that Hsp70 and TF can independently prevent biological harm (i.e., formation of insoluble species) generated by the I28D and M131D kinetic variants. The M131D variant was previously shown to act immediately post-translationally, by disrupting the relative kinetics of formation of soluble and insoluble ribosome-released gene products.[3] No kinetic data are currently available for the I28D variant. On the other hand, the fact that the chaperone-dependent results of Figure 4 are equivalent for I28D and M131D apoMb suggests that I28D variant may act similarly to M131D. Therefore, the key steps leading to apoMb-insoluble aggregate formation take place post-translationally for M131D, and possibly also for I28D. A proposed free-energy landscape matching the above concepts is discussed in a later section of this work.

Note that the TF chaperone is known to bind nascent proteins cotranslationally and this expectation is corroborated by previous experiments on ribosome-bound WT apoMb nascent chains (apoMb RNCs) in the presence of anti-TF antibodies.[25] Chaperones may therefore bind the nascent chain cotranslationally and then post-translationally address aggregation issues that arise upon release from the ribosome. In support of this idea, TF was found to keep interacting with nascent chains even after reaching a non-ribosome-bound state.[66] Additional future work is necessary to shed further light on this topic.

One major missing piece of information at this juncture is the fact that the composition of the soluble fraction is not known. For instance, this fraction may be entirely composed of native protein, or it may include additional, potentially self-associated soluble species. The sections below detail our efforts to further characterize the soluble fraction of ribosome-released newly synthesized protein chains.

**Insoluble and Soluble Fractions Generated upon Nascent-Chain Release from the Ribosome Are Kinetically Trapped Relative to Each Other.** Next, we examined whether the soluble and insoluble fractions populated by newly synthesized I28D and M131D apoMb are thermodynamically linked. To explore this concept, we took advantage of known thermodynamic models for nucleated polymerization, which were developed to describe aggregation processes in terms of reversible equilibria and phase transitions characterized by a constant critical concentration of monomers in equilibrium with the aggregates.[67] This formalism has been widely inspired by analogous developments targeting micelle formation at equilibrium in the context of the hydrophobic effect.[68] According to these models, the formation of two phases (e.g., amphiphilic monomers and micelles, soluble and insoluble molecules) only occurs once a critical concentration of monomer has been reached. The latter is denoted as critical micelle concentration[68] and critical protein concentration[5b] (or simply critical concentration[67]) in the case of micelles and proteins, respectively. As one goes beyond this critical total concentration of monomer in solution, more of the self-associated phase (e.g., micelle or insoluble aggregate) keeps forming at equilibrium, while the monomer concentration remains constant at its critical value. This formalism has been widely used to describe phase equilibria in biology, e.g., in the context of protein aggregation[22a,69] and protein/nucleic acid condensates.[70]

Briefly, Figure 5a shows the simple experimental design that was adopted to test this concept. In essence, we employed resuspension of the isolated insoluble fraction into a fresh cell-


https://doi.org/10.1021/acs.jpcb.2c08485
J. Phys. Chem. B XXXX, XXX, XXX−XXX

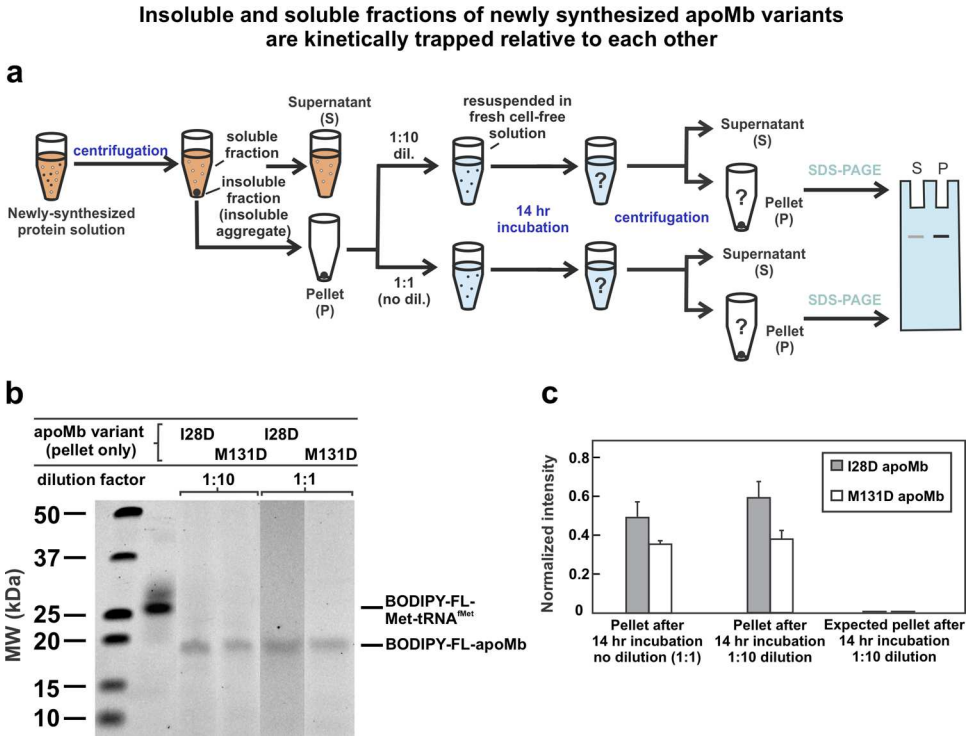


**Figure 5.** Insoluble apoMb variants are kinetically trapped from soluble states. (a) Schematic of the experimental procedure. N-terminally fluorophore-labeled protein-containing solutions are centrifuged followed by separation of soluble and insoluble fractions. The insoluble pellet (P) is resuspended in fresh cell-free solution, and the sample is incubated for about 14 h. After centrifugation, supernatant (S) and pellet (P) are isolated and visualized by low-pH SDS-PAGE and fluoroimaging. (b) Gel data shows the signal from the insoluble fractions of I28D and M131D apoMb upon dilution and incubation. The fluorophore-labeled apoMb and tRNA were visualized with a 488 nm excitation laser and a 500−550 nm band-pass emission filter (BPB1). Molecular weight markers were visualized with a 635 nm excitation laser and a 675 nm long-pass filter (LPR). Note that 10-fold more sample was loaded onto the gel for the 1:10 diluted samples, so that band intensities of diluted and non-diluted samples could be directly compared. (c) Itensity of the insoluble fraction of apoMb variants does not change upon incubation or dilution.

free solution devoid of newly synthesized variant apoMb gene products, followed by long-term incubation and centrifugation. If the soluble and insoluble fractions were thermodynamically linked, the insoluble fraction is expected to generate an overlaying equilibrium population of soluble fraction at the critical concentration, upon long-term incubation. In fact, we estimated that most of the pellet would dissolve if the soluble and insoluble fractions of newly synthesized proteins interconverted according to a thermodynamic equilibrium (see the Experimental Methods section and the SI for additional details). Given that no pellet dissolution was observed (Figure 5b,c), we conclude that the soluble and insoluble fractions of I28D and M131D apoMb are kinetically trapped relative to each other. Note that the absence or presence of ATP does not change the observed outcome (Supporting Figure S1). The presence of kinetic trapping is not unprecedented in biology.[5a] What is unique here is that the extent of kinetically trapped insoluble fraction (Figure 5) is found to be chaperone-concentration-dependent (Figure 4). Further, the trapping of soluble and insoluble fractions relative to each other is identified early in protein life, consistent with previous kinetic studies on WT and M131D apoMb.[3]

**Solubility Is Not Sufficient for Structural Accuracy: Newly Synthesized WT apoMb Generated in the Absence of Hsp70 and TF Chaperones Populates Soluble Aggregates, in Addition to Some Native State.** Soluble proteins are not necessarily structurally accurate, given that they may attain soluble misfolded states and(or) soluble aggregates, in addition to native monomers, upon release from the ribosome. Therefore, we set out to further explore the nature of the soluble fraction of newly synthesized apoMb in the absence and presence of the Hsp70 chaperone. Previous work employed 2D NMR in combination with SDS-PAGE and fluorescence to characterize the soluble fraction of WT apoMb generated in the cell-free-system environment in the absence of chaperones.[3] NMR in combination with SDS-PAGE showed that only 23.5% of the protein is biosynthesized in its native state, with the remaining 76.5% in slow exchange with the native conformation and spectroscopically undetectable.[3] This result revealed the presence of either (a) a very slow-tumbling species or (b) additional monomeric conformations in mutual intermediate exchange on the NMR chemical-shift timescale and in slow exchange with the native state.[3]

Fluorescence anisotropy decay in the frequency domain is a powerful tool to study protein conformation and dynamics,[33,35,63b,71] including events that take place upon release from the ribosome.[25,36] Application of this methodology to newly synthesized WT apoMb (Table 2, item 1) shows that the soluble fraction of newly synthesized wild-type apoMb includes very slow-tumbling species in the absence of chaperones, at even lower apoMb concentration than the NMR studies. This result lends support to the above interpretation (a) of the NMR results.

Next, we compared data collected via fluorescence anisotropy decays in the frequency domain under different conditions. We identified rotational correlation times ($\tau_c$) corresponding to local and global motions, as well as order


https://doi.org/10.1021/acs.jpcb.2c08485
J. Phys. Chem. B XXXX, XXX, XXX−XXX

**Table 2. Frequency-Domain Fluorescence Anisotropy Decay Parameters of Newly Cell-Free-Expressed (i.e., off the Ribosome) WT and Mutant apoMb in the Absence and Presence of Molecular Chaperones[a]**

| | timescale of motion (anisotropy decays)[d] | | | | | | | | |
|---|---|---|---|---|---|---|---|---|---|
| | slow (≥10 ns) | intermediate (0.5−2 ns) | | | fast (0−0.5 ns) | | | reduced $\chi^2$ | |
| system | $\tau_{c,S}$ (ns) | $\tau_{c,I}$ (ns) | $S_I$ | $\theta_I$ (deg) | $\tau_{c,F}$ (ns) | $S_F$ | $\theta_F$ (deg) | 2-component[e] | 3-component[e] |
| WT apoMb | | | | | | | | | |
| item 1: Δtig cf sys. + Hsp70 inhib. diluted[b] | 700 ± 200 | | | | 0.122 ± 0.004 | 0.25 ± 0.02 | 68.5 ± 0.8 | **0.47 ± 0.03** | 0.44 ± 0.04 |
| item 2: Δtig cf sys. + Hsp70 inhib.[b] | 260 ± 180 | | | | 0.104 ± 0.005 | 0.38 ± 0.01 | 59.6 ± 0.7 | **0.57 ± 0.06** | 0.37 ± 0.02 |
| item 3: WT cf sys. + 21 μM Hsp70[c] | 220 ± 140 | 0.91 ± 0.07 | 0.78 ± 0.01 | 32.5 ± 0.9 | 0.074 ± 0.008 | 0.57 ± 0.01 | 47.0 ± 0.8 | 1.5 ± 0.2 | **0.30 ± 0.03** |
| item 4: Δtig cf sys + 75 μM Hsp70[c] | 70 ± 21 | 0.7 ± 0.1 | 0.65 ± 0.05 | 42 ± 3 | 0.02 ± 0.02 | 0.79 ± 0.07 | 31 ± 6 | 5.0 ± 0.8 | **1.0 ± 0.2** |
| item 5: WT cf sys. + 75 μM Hsp70[b,c] | 62 ± 9 | 1.28 ± 0.09 | 0.76 ± 0.02 | 33 ± 2 | 0.080 ± 0.005 | 0.629 ± 0.006 | 43.2 ± 0.4 | 2.8 ± 0.4 | **0.37 ± 0.03** |
| item 6: WT cf sys. + 75 μM Hsp70 + Hsp70 inhib. Added post-translationally[b,c] | 44 ± 5 | 1.25 ± 0.07 | 0.72 ± 0.02 | 37 ± 1 | 0.07 ± 0.01 | 0.62 ± 0.01 | 43.9 ± 0.9 | 3.2 ± 0.2 | **0.39 ± 0.07** |
| item 7: WT cf sys. + 75 μM Hsp70, diluted[b,c] | 34 ± 2 | 1.3 ± 0.1 | 0.80 ± 0.01 | 30.6 ± 0.1 | 0.108 ± 0.008 | 0.58 ± 0.01 | 46.8 ± 0.7 | 1.65 ± 0.07 | **0.4 ± 0.1** |
| item 8: purified apoMb resuspended in RNC solution[f] | 10 ± 2 | | | | 0.103 ± 0.006 | 0.67 ± 0.04 | 48 ± 3 | **1.3 ± 0.3** | 0.7 ± 0.1 |
| I28D apoMb | | | | | | | | | |
| WT cf sys + 75 μM Hsp70 | | | | | | | | | |
| item 9: spatially biased/long-lifetime species | 240 ± 80 | | | | 0.17 ± 0.01 | 0.63 ± 0.01 | 43.0 ± 0.5 | 1.1 ± 0.5 | 0.5 ± 0.2[g] |
| item 10: dynamic/short-lifetime species | | | | | 0.19 ± 0.01 | 0 | 180 | 1.1 ± 0.5 | 0.5 ± 0.2[g] |

[a]Symbols are as follows: Δtig, strain lacking gene encoding trigger factor (TF) chaperone; WT, wild-type; cf sys., cell-free system; Hsp70 inhib., peptide that inhibits Hsp70..[1] [b]Anisotropy decay parameters for items 1,2,5, 6, and 7 reproduced with permission from ref 3. Copyright 2020 American Chemical Society. [c]For the 21 μM and 75 μM Hsp70 conditions, 0.04−12 μM DnaJ and 19 μM GrpE were also added. [d]The subscripts S, I, and F refer to slow global motions (μs), intermediate local motions (ns), and fast local motions (sub-ns), respectively. The symbols $\tau_{c,S}$, $\tau_{c,I}$, and $\tau_{c,F}$ denote the rotational correlation times. $S_I$, and $S_F$ are the order parameters, and $\theta_I$ and $\theta_F$ are the cone semiangles that describe the spatial confinement of the tumbling motions. Uncertainty values for $\tau_c$, S, and $\theta_c$ are reported as either propagated error or standard error (SE, whichever value was larger), out of 2−7 independent experiments. [e]The reduced $\chi^2$ values listed in the table are the average and SE for all independent experiments. Three-component models were selected instead of two-component models if the reduced $\chi^2$ for the three-component fit was ≥2.5 times smaller than the reduced $\chi^2$ for the two-component model. Accordingly, a three-component model was selected for WT apoMb produced in the presence of chaperones, and a two-component model was selected for WT apoMb produced in the absence of chaperones. The chosen number of components for any given experimental item is shown in bold. [f]Data generated from reprocessing of anisotropy decay data originally reported in Ziehr et al.[37] Reprocessing procedure described in Supporting Methods. [g]Reduced $\chi^2$ values for associative model. Data are reported as avg ± SE.



https://doi.org/10.1021/acs.jpcb.2c08485
J. Phys. Chem. B XXXX, XXX, XXX−XXX

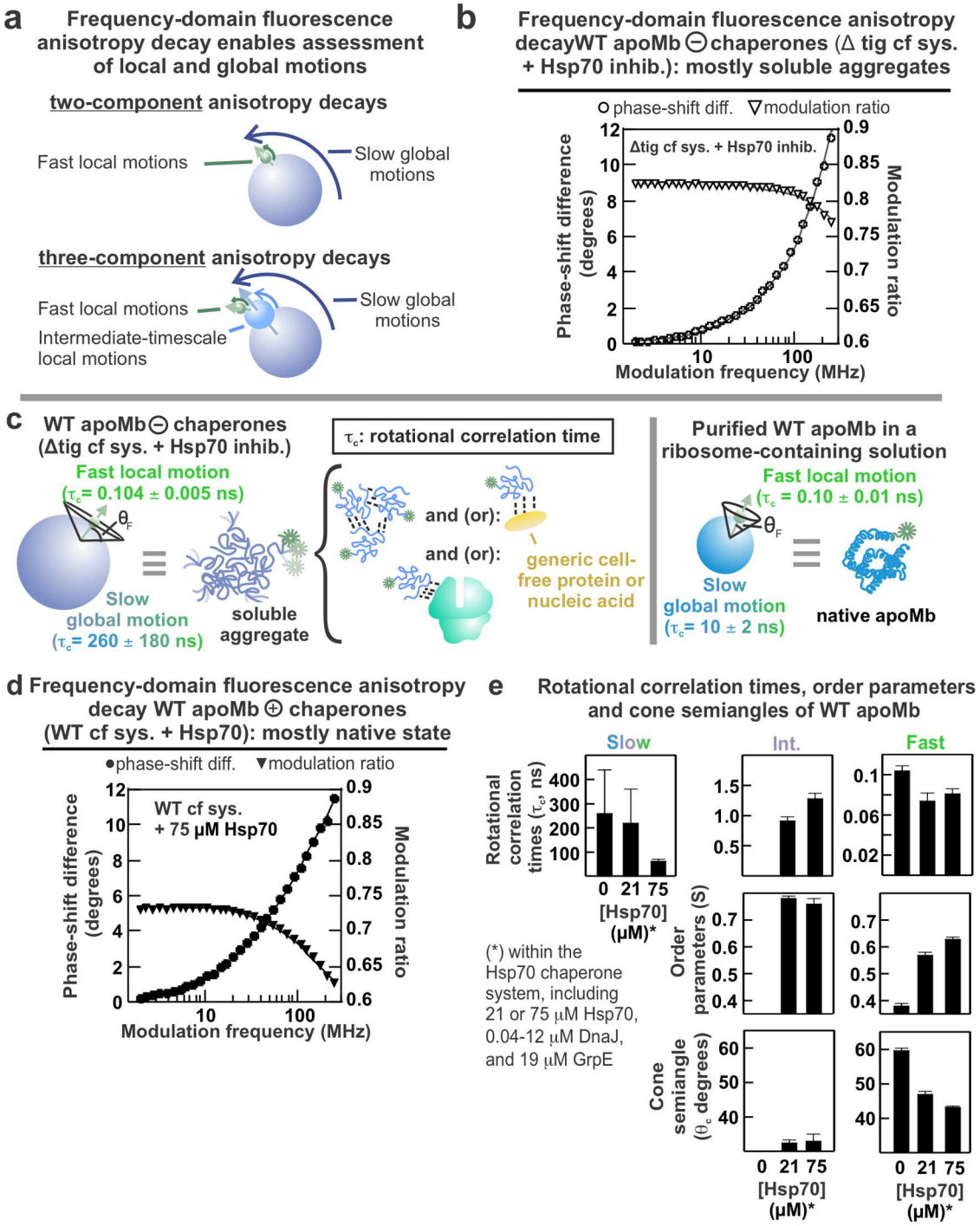


**Figure 6.** apoMb generated in the absence or presence of Hsp70 has different structural features. (a) Frequency-domain fluorescence anisotropy decays can resolve up to three rotational motions. (b) Representative anisotropy decay data for apoMb (0.3 ± 0.2 $\mu$M) synthesized in the absence of TF and KJE chaperones. (c) $\tau_c$ values for apoMb synthesized in the absence of chaperones are consistent with soluble aggregates (left) and larger than $\tau_c$ values for purified monomeric protein (right). (d) Representative anisotropy decay data for apoMb (0.3 ± 0.2 $\mu$M) synthesized in the presence of 75 $\mu$M Hsp70. (e) Rotational correlation times (top), order parameters (S, middle), and cone semiangles (bottom) for the global and local motions of apoMb synthesized in the presence of different chaperone concentrations. Error bars denote propagated error or the standard error for $n$ = 2−7 (whichever value was larger). Some of these data are also presented in Table 2 of Addabbo et al.[3] For the 21 and 75 $\mu$M Hsp70 conditions, 0.04−12 $\mu$M DnaJ and 19 $\mu$M GrpE were also present. For 0 $\mu$M chaperones, a Δtig cell-free was used with 0.4 mM Hsp70 inhibitor.[1]

parameters and matching spatial amplitudes of local motions. As shown in Figure 6a, $\tau_c$ values are proportional to the size of the corresponding tumbling species, either the entire particle or portions of it that are covalently linked to the N-terminal BODIPY-FL fluorophore. This technique can resolve up to three different $\tau_C$ values within a sample, as long as the motions are independent[36] and bear sufficiently different timescales (typically by ≥5-fold).[72] Figure 6b displays representative fluorescence anisotropy decay data for WT apoMb made in the absence of the Hsp70 chaperone. Newly synthesized WT apoMb produced in the absence of molecular chaperones within the cell-free system has a large rotational


https://doi.org/10.1021/acs.jpcb.2c08485
J. Phys. Chem. B XXXX, XXX, XXX−XXX

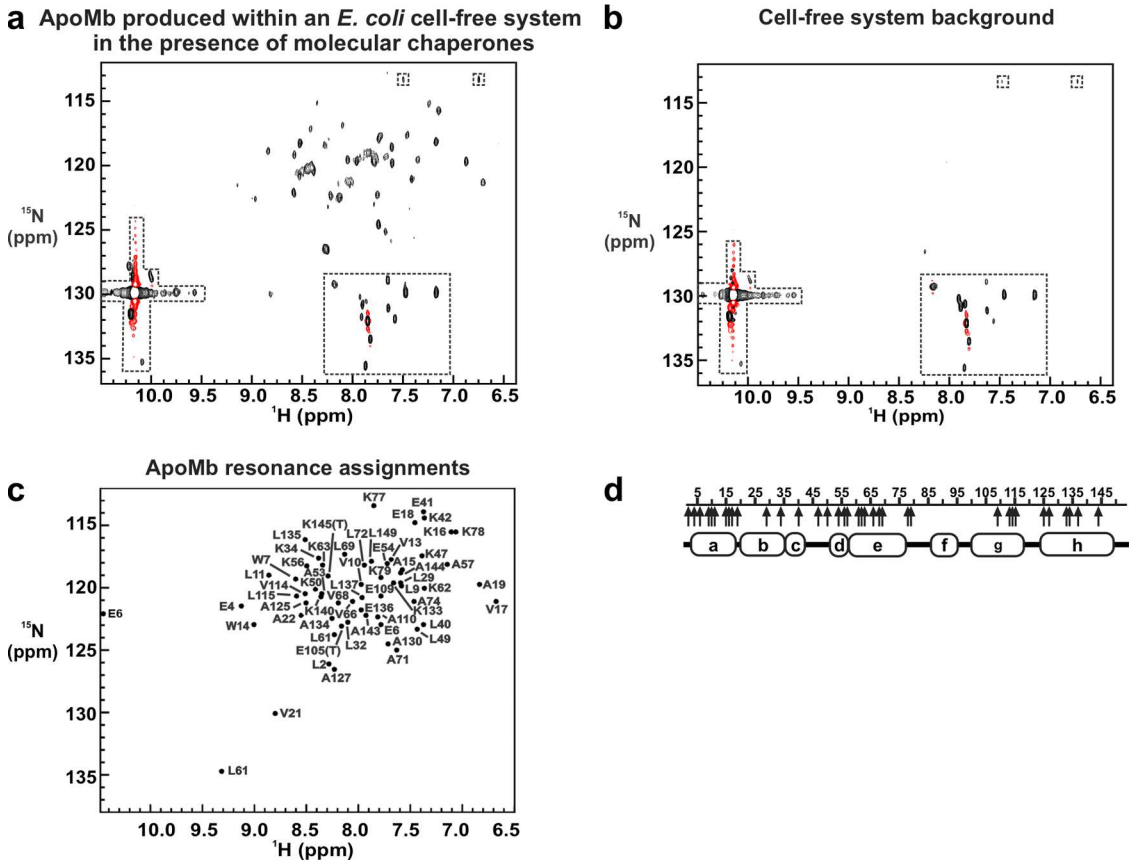


**Figure 7.** WT apoMb is folded and soluble aggregates are minimized when produced off ribosome in the presence of chaperones. $^{1}$H, $^{15}$N HSQC NMR spectra of selectively labeled apoMb ($^{15}$N-labeled A, E, L, K, V, and $^{13}$C- and $^{15}$N-labeled W) generated by transcription-translation in an *E. coli* cell-free system.[4] All data were immediately collected following transcription-translation and contained levels of chaperones naturally present in the cell-free system ([apoMb] = 7.3 $\mu$M, [Hsp70] = 0.5 $\mu$M, [DnaJ] = 0.04 $\mu$M, [GrpE] = 0.05 $\mu$M, [TF] = 0.2 $\mu$M).[3] All dashed boxes indicate resonances present in the negative control, denoting products of amino acid metabolism[7] and free tryptophan (a) Spectrum of cell-free expressed apoMb. Black, unboxed resonances are consistent with resonances of apoMb native state and have been tentatively assigned.[10] (b) Cell-free reaction in the absence of T7 RNA polymerase (negative control). (c) Simulated 2D $^{1}$H, $^{15}$N HSQC spectrum of apoMb based on known assignments.[10] (d) Labeled amino acids (arrows) and $\alpha$-helical secondary structure of native WT apoMb.

correlation time ($\tau_c$) for global tumbling. Namely: $\tau_c$ = 260 ± 180 in cell-free systems and $\tau_c$ = 700 ± 200 ns in cell-free systems diluted 10−13-fold (items 1 and 2 in Table 2). Importantly, the latter rotational correlation time is significantly larger than the corresponding value obtained for independently purified apoMb ($\tau_c$ = 10 ± 2 ns, item 8 of Table 2) mixed in a solution containing ribosomes at a comparable concentration to ribosome concentration of crude cell-free systems (one-tailed Student's *t*-test, Table S5). Therefore, WT apoMb made within the *E. coli* cell-free environment in the absence of chaperones includes a slow-tumbling species with a large $\tau_c$ of 200−700 ns, which we define here as soluble aggregate. The volume of this species is estimated to be 28- to 90-fold larger than monomeric apoMb (Table S6). Note that the large $\tau_c$ uncertainty of newly synthesized apoMb in the absence of chaperones reflects the fact that it is difficult to resolve rotational motions substantially larger than the fluorescence lifetime of the fluorophore (~5 ns for BODIPY-FL).

As pictorially illustrated in Figure 6c, the term soluble aggregate encompasses homo-aggregates formed from multiple mutually interacting apoMb chains, hetero-aggregates composed of apoMb in complex with the ribosome, or hetero-aggregates featuring apoMb interacting with other cellular proteins. Additional work is necessary to shed further light on the structural details of the soluble aggregate. Importantly, the size of this species decreases when protein expression is carried out in the presence of molecular chaperones (see next section). Therefore, the large $\tau_c$ observed for soluble aggregates is not merely the result of nonspecific binding to cell-free components, though this effect may partially contribute to the observed $\tau_c$. Note that the $\tau_c$ of WT apoMb does not significantly change upon addition of the KLR-70 Hsp70 peptide inhibitor[1] after translation (Table 2 item 6). Therefore, WT apoMb is not bound to Hsp70 at equilibrium.

Experiments employing fluorophores with long lifetimes, including DAOTA (lifetime = 16.2 ns) and ADOTA (lifetime = 19.2 ns)[73] were also carried out (data not shown). These investigations, however, were unsuccessful due to poor protein labeling efficiencies and(or) due to nonspecific binding of the long-lifetime probes to cell-free-system components. Additional strategies to better understand the nature of the soluble aggregate, including mass photometry and ribosome immunoprecipitation assays to selectively eliminate 70S ribosomes, led to no further usable information (SI text and Table S7).

At this juncture, it is helpful to recapitulate the results of NMR/SDS-PAGE and fluorescence anisotropy. As already discussed, previous 2D NMR data acquired on cell-free


https://doi.org/10.1021/acs.jpcb.2c08485
J. Phys. Chem. B XXXX, XXX, XXX−XXX

expressed WT apoMb within a chaperone-free cell-free environment under the same experimental conditions show that some native WT apoMb is present in solution.[3] On the other hand, fluorescence anisotropy decay data collected at even lower concentrations show that a slow-tumbling species is also present in solution. Therefore, we conclude that cell-free expression of WT apoMb in the absence of chaperones yields a mixture of native state and soluble aggregates. Phasor plot analysis, shown in a later section of this work, sheds additional light on the relative populations of these two components.

**Increasingly High Hsp70 Chaperone Concentrations Lead to Improved Structural Accuracy of Newly Synthesized WT apoMb.** Previous fluorescence anisotropy decay data collected in the presence of the Hsp70 chaperone showed that the observed global size of the tumbling particles gets smaller in the presence of the Hsp70 chaperone system.[3] Here, we share the same fluorescence anisotropy data but display them in a more comprehensive fashion, including representative raw phase-modulation profiles, and add some new results on data collected at one additional Hsp70 concentration (21 mM). In this way, we more directly address trends related to the presence of increasing concentrations of the Hsp70 chaperone. Some representative raw data are shown in Figure 6d, and chaperone-dependence trends are illustrated in Figure 6 and Table 2.

Items 4−7 of Table 2 show that apoMb biosynthesized in the presence of 75 $\mu$M Hsp70 has a smaller global $\tau_c$ than apoMb generated in the absence of chaperones. Interestingly, the latter species fits best to a three-component anisotropy decay. We tentatively ascribe the 1.3 ns intermediate-timescale motion to a small compact N-terminal region, likely including some independently tumbling A-helix residues.

In addition, the samples generated in the absence and presence of Hsp70 show different local dynamics. The fast (sub-ns, $\tau_C \sim 0.1$ ns) local motions of WT apoMb are diagnostic of motions of the first N-terminal residues of the newly synthesized protein chain, based on tumbling-rate arguments and on the Stokes−Einstein−Debye equation.[25] Interestingly, in the presence of the Hsp70 chaperone, newly synthesized apoMb exhibits confined dynamics characterized by a relatively small cone semiangle for the fast sub-ns local motions and by a large order parameter (Figure 6e and Table 2 items 3−7).[36] Conversely, apoMb synthesized in the absence of Hsp70 exhibits N-terminal local motions of slightly wider amplitude (Figure 6e and Table 2, items 1 and 2). These differences in the amplitude of the motions of the protein N termini are likely related to the different local microstructure of WT apoMb in its monomeric and soluble-aggregate forms.

As shown in Figure 6e and Table 2, the presence of increasing concentrations of the Hsp70 chaperone system leads to an apparent decrease in the observed size of newly synthesized apoMb, as testified by the increasingly lower $\tau_c$ values. However, the observed $\tau_c$ at physiologically relevant concentrations of the Hsp70 chaperone system (34−62 ns, Table 2) is still larger than expected for a 100% population of folded monomeric protein (Table 2, item 8). This result suggests that either smaller-size aggregates and(or) a lower fraction of same-size aggregates are still present in the system, even at 75 $\mu$M Hsp70 concentration.

The overall idea that chaperones increase the percent native state, but do not fully prevent soluble aggregate formation is supported by the 2D NMR spectroscopy/SDS-PAGE data in the presence of Hsp70 and TF (Figure 7), in combination with known data under chaperone-free conditions.[3] As summarized in Table 3, the percent of NMR-detected native state increases at higher chaperone concentrations. As already discussed in the previous section, NMR/SDS-PAGE is a powerful approach because it provides a direct assessment of the concentration of newly synthesized native apoMb in the cell-free environment, even in the presence of some spectroscopically undetectable slow-tumbling apoMb.

**Table 3. Percent Native State of Newly Synthesized (Off-Ribosome) Wild-Type apoMb, Detected by 2D Heteronuclear NMR Spectroscopy ($^1$H−$^{15}$N HSQC) in Combination with SDS-PAGE at Different Chaperone Concentrations**

| apoMb concentration ($\mu$M) | Hsp70 concentration ($\mu$M) | TF concentration ($\mu$M) | percent native state[a] | total NMR data collection time (h) |
|---|---|---|---|---|
| 59.8 | 0 | 0 | 23.5 ± 0.9 | 41 |
| 7.3 | 0.5 | 0.2 | 30 ± 2 | 87 |

[a]Percent native states are reported as average ± SE and were determined from seven clearly resolved apoMb resonances (see the Experimental Methods section and Supporting Table S2). The error in resonance volume was propagated via standard procedures,[74] to deduce the error in the percent native state defined according to eq 10.

The combination of fluorescence anisotropy decays and NMR/SDS-PAGE suggests that apoMb produced in the presence of Hsp70 comprises a mixture of native protein and a slow-tumbling version of the same protein. Additional data derived from fluorescence lifetime phasor plots further support this interpretation and shed additional details on the relative proportions of the two species (see next section).

In principle, instead of being an authentic soluble aggregate, newly synthesized apoMb may simply undergo weak transient interactions with other species that slow down its tumbling motion within the complex cell-free mixture. However, weak and fast interactions on the NMR chemical-shift timescale are ruled out because these interactions would broaden the native-state apoMb resonances, and no line-broadening was observed (Figure 7).

The presence of soluble aggregates is also consistent with fluorescence emission spectra of newly synthesized WT apoMb in the cell-free environment. These spectra show a small reproducible blueshift for the protein produced in the absence of chaperones, relative to chaperone-free conditions (Supporting Figure S2). This result supports the presence of a more nonpolar environment, possibly due to a larger fraction of soluble aggregate, for the newly synthesized protein produced in the absence of chaperones.

Interestingly, the $\tau_c$ of the sample generated in the presence of chaperones gets reproducibly smaller upon sample dilution (Table 2 items 5 and 7). The decrease in viscosity upon dilution is partially responsible for this change in $\tau_c$ (33% of the effect), as testified by the experimental microscale-volume viscosity measurements reported in Table 4. Small changes in the degree of soluble-aggregate levels may also contribute to the observed $\tau_c$ variations. The estimated protein hydrated volume is similar for both samples (Supporting Table S6). Further, as shown in Table 5 (items 5 and 7), fluorescence lifetime changes are negligible upon dilution, suggesting similar fractions of native state and soluble aggregates, in the presence


https://doi.org/10.1021/acs.jpcb.2c08485
J. Phys. Chem. B XXXX, XXX, XXX−XXX

**Table 4. Viscosity of Undiluted and Diluted Cell-Free Systems[a]**

| system | viscosity (mPa·s)[b] |
|---|---|
| item 1: Δtig cf sys. + Hsp70 inhib. diluted | 0.940 ± 0.005 |
| item 2: Δtig cf sys. + Hsp70 inhib. | 1.13 ± 0.02 |
| item 5: WT cf sys. + 75 μM Hsp70[c] | 1.11 ± 0.01 |
| item 7: WT cf sys. + 75 μM Hsp70, diluted[c] | 0.940 ± 0.004 |

[a]Symbols are as follows: Δtig, strain lacking gene encoding trigger factor (TF) chaperone; WT, wild-type; cf sys., cell-free system; Hsp70 inhib., peptide that inhibits Hsp70.[1] [b]The viscosity values are the average and SE for three independent experiments at shear rates of 1500 and 8000 $s^{-1}$, respectively. [c]For the 75 μM Hsp70 conditions, 0.04−12 μM DnaJ and 19 μM GrpE were also added.

of Hsp70 and TF chaperones (see also phasor analysis in next section). We conclude that undiluted and diluted newly synthesized apoMb samples prepared in Hsp70- and TF-containing solutions include similar fractions of monomeric folded protein.

**Lifetime Phasors Enable Estimating the Fraction of Newly Synthesized WT apoMb Native State and Soluble Aggregates at Different Chaperone Concentrations.** Fluorescence lifetimes are powerful probes of the environment. Representative raw data for fluorescence lifetimes of WT apoMb generated in the absence and presence of chaperones are shown in Figure 8a. The N-terminal BODIPY-FL fluorophore within the protein has different fluorescence lifetimes in the absence and presence of chaperones, as shown in Figure 8b and Table 5. These differences are far greater than those observed for the free dye in the absence or presence of chaperones (Figure 8b). This result points to a different environment experienced by WT apoMb in the absence and presence of chaperones.

Phasor analysis of fluorescence lifetime data provides additional key information. Lifetime phasors are powerful probes of relative fractions of different components in mixtures.[34,75] If different experimental conditions generate phasor points that lie along a single line, lifetime phasors support the presence of different populations of mixture components.[34,75] S and G phasor values were computed from phase shift and modulation data at 23.08 MHz modulation frequency data collected for apoMb expressed with different molecular-chaperone levels. First, we found that the phasors of the free BODIPY-FL dye (in the cell-free environment) lie very close to the universal circle (Figure 8c, see also fluorescence lifetimes of the free dye in Table 5). In contrast, all phasors of cell-free synthesized WT apoMb produced in the presence of different concentrations of TF and Hsp70 chaperones lie along a straight line within the universal circle (Figure 8c). This result strongly supports the presence of different relative amounts of two noninteracting populations, under the different chaperone conditions.[34] Given the fluorescence anisotropy and NMR/SDS-PAGE results, we ascribe these variable populations to native WT apoMb monomers and soluble aggregates. By explicitly plotting the phasors of 100% monomeric apoMb and by estimating the percent of soluble aggregates from the NMR experiments in the absence of chaperones,[3] we were able to estimate the maximum fractions of soluble aggregates populated under a variety of different conditions, including different concentrations of TF and Hsp70 chaperones, as shown in Figure 8c and Table 6. The emerging picture is extremely informative. Namely, larger concentrations of TF and Hsp70 chaperones lead to a decrease in the fraction of soluble aggregates. The presence of TF in solution decreases the required concentration of Hsp70 to reach any given fraction of native protein in the cell-free mixture.

**Table 5. Time-Resolved Fluorescence Lifetime of apoMb Produced in the Presence of Variable Chaperone Concentrations[a]**

| | fluorescence lifetimes and related parameters[b] | | | | avg fluorescence lifetime (ns)[d] |
|---|---|---|---|---|---|
| | long | | short | | |
| | fraction[c] | $L_1$ (ns) | fraction[c] | $L_2$ (ns) | |
| | WT apoMb | | | | |
| item 1: Δtig cf sys. + Hsp70 inhib. diluted | 0.51 ± 0.02 | 5.08 ± 0.07 | 0.47 ± 0.02 | 1.77 ± 0.03 | 3.4 ± 0.1 |
| item 2: Δtig cell strain + Hsp70 inhib. | 0.59 ± 0.01 | 4.82 ± 0.04 | 0.39 ± 0.01 | 1.76 ± 0.04 | 3.52 ± 0.05 |
| item 3: WT cf sys. + 21μM Hsp70[e] | 0.67 ± 0.02 | 5.13 ± 0.04 | 0.30 ± 0.02 | 1.79 ± 0.05 | 4.0 ± 0.1 |
| item 4: Δtig cf sys + 75 μM Hsp70[e] | 0.75 ± 0.03 | 4.9 ± 0.2 | 0.17 ± 0.03 | 1.3 ± 0.2 | 3.9 ± 0.2 |
| item 5: WT cf sys. + 75 μM Hsp70[e] | 0.76 ± 0.01 | 5.15 ± 0.04 | 0.22 ± 0.01 | 1.79 ± 0.04 | 4.29 ± 0.04 |
| item 6: WT cf sys. + 75 μM Hsp70 + Hsp70 inhib. added post-translationally[e] | 0.76 ± 0.01 | 5.07 ± 0.03 | 0.21 ± 0.01 | 1.74 ± 0.08 | 4.25 ± 0.07 |
| item 7: WT cf sys. + 75 μM Hsp70, diluted[e] | 0.75 ± 0.01 | 5.37 ± 0.03 | 0.22 ± 0.01 | 1.85 ± 0.05 | 4.47 ± 0.07 |
| item 8: purified apoMb resuspended in RNC solution | 0.95 ± 0.02 | 5.7 ± 0.1 | 0.04 ± 0.02 | 2.0 ± 0.1 | 5.53 ± 0.08 |
| | I28D apoMb | | | | |
| items 9−10: WT cf sys. + 75 μM Hsp70 | 0.67 ± 0.01 | 5.5 ± 0.2 | 0.31 ± 0.01 | 1.9 ± 0.1 | 4.2 ± 0.2 |
| | BODIPY-FL Fluorophore Controls | | | | |
| item 11: BODIPY-FL dye in Δtig cf sys. + Hsp70 inhib. | 0.971 ± 0.007 | 5.22 ± 0.02 | 0.022 ± 0.006 | 1.8 ± 0.4 | 5.12 ± 0.04 |
| item 12: BODIPY-FL dye in WT cf sys. + 75 μM Hsp70 | 0.978 ± 0.002 | 5.36 ± 0.006 | 0.016 ± 0.002 | 1.66 ± 0.01 | 5.27 ± 0.01 |

[a]Symbols are as follows: Δtig, strain lacking gene encoding trigger factor (TF) chaperone; WT, wild-type; cf sys., cell-free system; Hsp70 inhib., peptide that inhibits Hsp70[1]; $L_1$ and $L_2$, fluorescence lifetimes. [b]Fluorescence lifetime data were fit to two fluorescence lifetimes ($L_1$ and $L_2$) and a third fictitious lifetime (0.001 ns) to account for small contributions from scattering. [c]Fraction denotes the fractional contribution of each lifetime to the total fluorescence decay. [d]An average (avg) fluorescence lifetime, weighted by the fractional contribution of $L_1$ and $L_2$ is further displayed. Error bars are the propagated error or standard error (SE) for 2−7 independent experiments. The larger of the two errors was selected. [e]For the 21 and 75 μM Hsp70 conditions, 0.04−12 μM DnaJ and 19 μM GrpE were also added.


https://doi.org/10.1021/acs.jpcb.2c08485
J. Phys. Chem. B XXXX, XXX, XXX−XXX

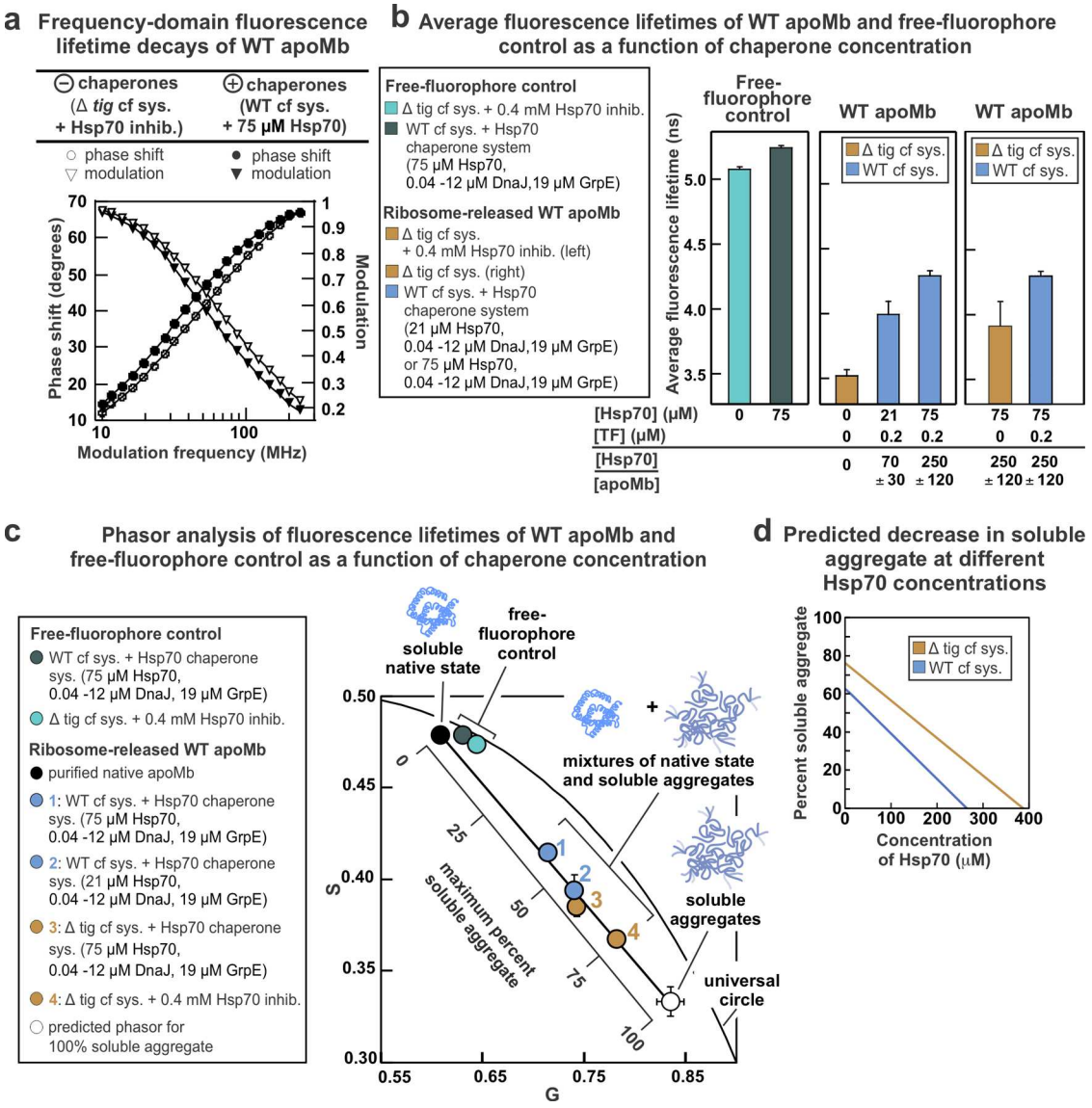


**Figure 8.** Hsp70 chaperone system increases the structural accuracy of WT apoMb. (a) Representative frequency-domain fluorescence lifetime decay data for apoMb generated in the absence and presence of KJE and TF chaperones. (b) Average fluorescence lifetimes of apoMb (0.3 ± 0.2 $\mu$M) and free BODIPY-FL fluorophore in cell-free systems containing different chaperone concentrations. Error bars denote either propagated error or standard error for $n = 2-7$ (whichever value was larger). (c) Fluorescence lifetime phasor plot at 23.08 MHz modulation frequency for free BODIPY-FL fluorophore and apoMb in cell-free systems containing different KJE and TF chaperone concentrations. Error bars denote propagated error or standard error for $n = 2-7$. All errors in G and S not seen are too small to be visualized on the plot. Some phasor plot points were also shown in the Supporting Material of Addabbo et al.[3] (d) Predicted percent of WT apoMb-soluble aggregate generated with different chaperone concentrations. For the 21 and 75 $\mu$M Hsp70 conditions, 0.04−12 $\mu$M DnaJ and 19 $\mu$M GrpE were also added.

Interestingly, physiologically relevant concentrations of the Hsp70 chaperone system are not sufficient to generate 100% native protein. As shown in Figure 8d, the projected concentrations of Hsp70 required to eliminate the presence of WT apoMb-soluble aggregates ($x$-axis intercept) exceed by far physiologically relevant concentrations of this chaperone, even in the presence of TF. This important result shows that cell-relevant concentrations of TF and Hsp70 chaperones are not sufficient to prevent the formation of soluble aggregates of all proteins.

In the specific case of the WT sperm-whale apoMb model protein analyzed here, this result may be a consequence of the fact that this protein is produced in the presence of heme, in Nature. This cofactor is expected to contribute beyond the action of molecular chaperones, to generate native state devoid of soluble aggregates.[76] Given that our cell-free systems were heme-free, this additional form of folding assistance was absent in our experiments.

**Hsp70 Acts Early on in Client-Protein Life to Grant Structural Accuracy to Newly Synthesized Proteins.** Hsp70 acts on nascent proteins co- and/or immediately post-translationally because the $\tau_c$ and phasor coordinates of WT apoMb do not significantly change upon the addition of the KLR-70 Hsp70 peptide inhibitor[1] well after translation has been completed (Table 2, item 6, Supporting Figure S3). Therefore, WT apoMb is not bound to Hsp70 after translation, and Hsp70 primarily interacts with newly synthesized proteins before they complete their folding. In addition, further incubation of either WT[3] apoMb or its I28D variant (see the Fluorescence Lifetime and Anisotropy Decay section) for


https://doi.org/10.1021/acs.jpcb.2c08485
J. Phys. Chem. B XXXX, XXX, XXX−XXX

**Table 6. Summary of Estimated Populations of Native and Aggregated States for WT and I28D apoMb made in the Presence of Different Concentrations of the Hsp70 Chaperon System**

| protein | Hsp70 concentration ($\mu$M)[a] | estimated percent native and aggregated states[b] | |
|---|---|---|---|
| WT apoMb | 0 | insoluble aggregate | 3 ± 1 |
| | | soluble aggregate | 74 ± 1 |
| | | native | 23 ± 1 |
| WT apoMb | 21 | insoluble aggregate | 3 ± 2 |
| | | soluble aggregate | 57 ± 11 |
| | | native | 40 ± 8 |
| WT apoMb | 75 | insoluble aggregate | 3 ± 1 |
| | | soluble aggregate | 44 ± 6 |
| | | native | 53 ± 7 |
| I28D | 75 | insoluble aggregate | 13 ± 2 |
| | | soluble aggregate | 59 ± 2 |
| | | dynamic conformation | 28 ± 1 |

[a]For the 21 and 75 $\mu$M Hsp70 conditions, a WT cell-free system was employed and 0.04−12 $\mu$M DnaJ and 19 $\mu$M GrpE were added. For the 0 $\mu$M Hsp70 condition, a Δtig cell-free was employed and 0.4 mM Hsp70 inhibitor[1] was added. [b]Error bars are the propagated error.

up to ca. 1 h does not lead to any changes in the rotational properties of the newly synthesized protein.

**Working Model: Hsp70 and TF Lead to a Decrease in the Fraction of Soluble Aggregates Generated upon Newly Synthesized Protein Expression.** The results from the previous sections show that increasing concentrations of the Hsp70 and TF chaperone systems decrease the extent of soluble-aggregate formation in a concentration-dependent manner. This concept is schematically illustrated in Figure 9a,b. Note that the chaperone concentrations required to prevent soluble aggregate formation are higher than those required to prevent insoluble aggregate formation, as shown upon comparing the data in Figures 4, 8, and 10. More details on this item are provided in the next section.

**Different Protein Sequences Have Distinct Hsp70-Chaperone Requirements for the Prevention of Soluble-Aggregate Formation.** Next, we focused on the newly synthesized I28D apoMb variant to gain additional insights into the nature of the soluble fraction populated by this species upon release from the ribosome. Fluorescence depolarization in the frequency domain of newly synthesized proteins was carried out directly within the cell-free environment. The WT and I28D variants were compared side-by-side, and representative fluorescence lifetime and fluorescence depolarization decay profiles are shown in Figure 10a,b, respectively. Fluorescence anisotropy decay parameters deduced from curve fitting are also shown in Table 2. All data were collected in the presence of high concentrations of the Hsp70 chaperone (75 $\mu$M) and its cochaperones (at ca. K/J/E 5:1:2 molar ratios). The ribosome-released I28D variant fits best to an associative fluorescence anisotropy decay model.[32,63a,77] Several associative models were tried and the simplest one that provides excellent data fitting is shown in Figure 10c (see also Table 2). Briefly, this model comprises a slow-tumbling aggregate ($\tau_{c1}$ = 240 ± 80 ns) with a flexible N terminus ($\tau_{c2}$ = 0.17 ± 0.01 ns) as well as an additional species with an extremely dynamic isotropically tumbling N terminus ($\tau_{c3}$ = 0.19 ± 0.01 ns). The latter species may well be an aggregate with an extremely flexible N terminus or an overall

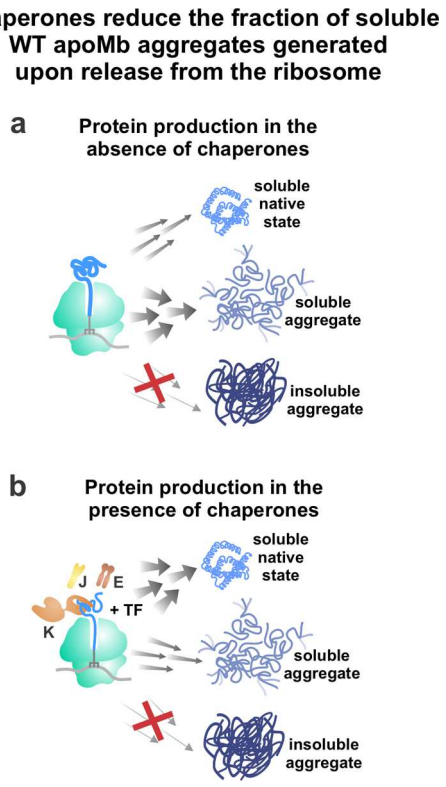


**Figure 9.** Quantitative concentrations of KJE are required to increase structural accuracy of apoMb. (a) Synthesis in the absence of KJE (Δtig cell-free system plus 0.4 mM Hsp70 inhibitor[1]) results in 73.5 ± 0.9% soluble aggregate when apoMb concentration is 59.8 $\mu$M. (b) Protein is channeled to its native state when synthesized in the presence of KJE (0.3 ± 0.2 $\mu$M apoMb, 75 $\mu$M Hsp70, 0.04−12 $\mu$M DnaJ, 19 $\mu$M GrpE, and 0.2 $\mu$M TF), enabling production of at least 53 ± 7% native state. While apoMb can be synthesized in the absence of chaperones and remain fully soluble, there is a quantitative requirement for KJE concentrations for structural accuracy.

highly flexible monomer. This concept is pictorially illustrated in Figure 10d, which also lists the relative populations of the two species.

Interestingly, the large aggregate with $\tau_{c1}$ = 240 ± 80 ns formed by I28D apoMb has different characteristics from the soluble aggregate detected in the case of WT apoMb, in terms of N-terminal amplitude of motions (Table 2) and lifetime values (Table 5). Therefore, the soluble aggregates of I28D and WT apoMb likely have a different structure as well, in addition to different dynamic properties.

Finally, the data of the fluorescence lifetime phasor plot of Figure 10e shows that incubation of the I28D apoMb within the cell-free-system environment leads to no changes in solution composition as a function of time. Therefore, the two I28D apoMb-soluble species detected in solution (soluble aggregate and highly dynamic species) are either in equilibrium or kinetically trapped relative to each other.

In all, the data in Figure 10 demonstrate that different protein sequences have different chaperone requirements for solubility and structural accuracy. Importantly, we show that even single-point mutations can change the chaperone concentration required to prevent insoluble and soluble aggregation. While I28D is mostly soluble at ∼75 $\mu$M Hsp70, this chaperone concentration is not sufficient to prevent soluble aggregation. This result is consistent with


https://doi.org/10.1021/acs.jpcb.2c08485
J. Phys. Chem. B XXXX, XXX, XXX−XXX

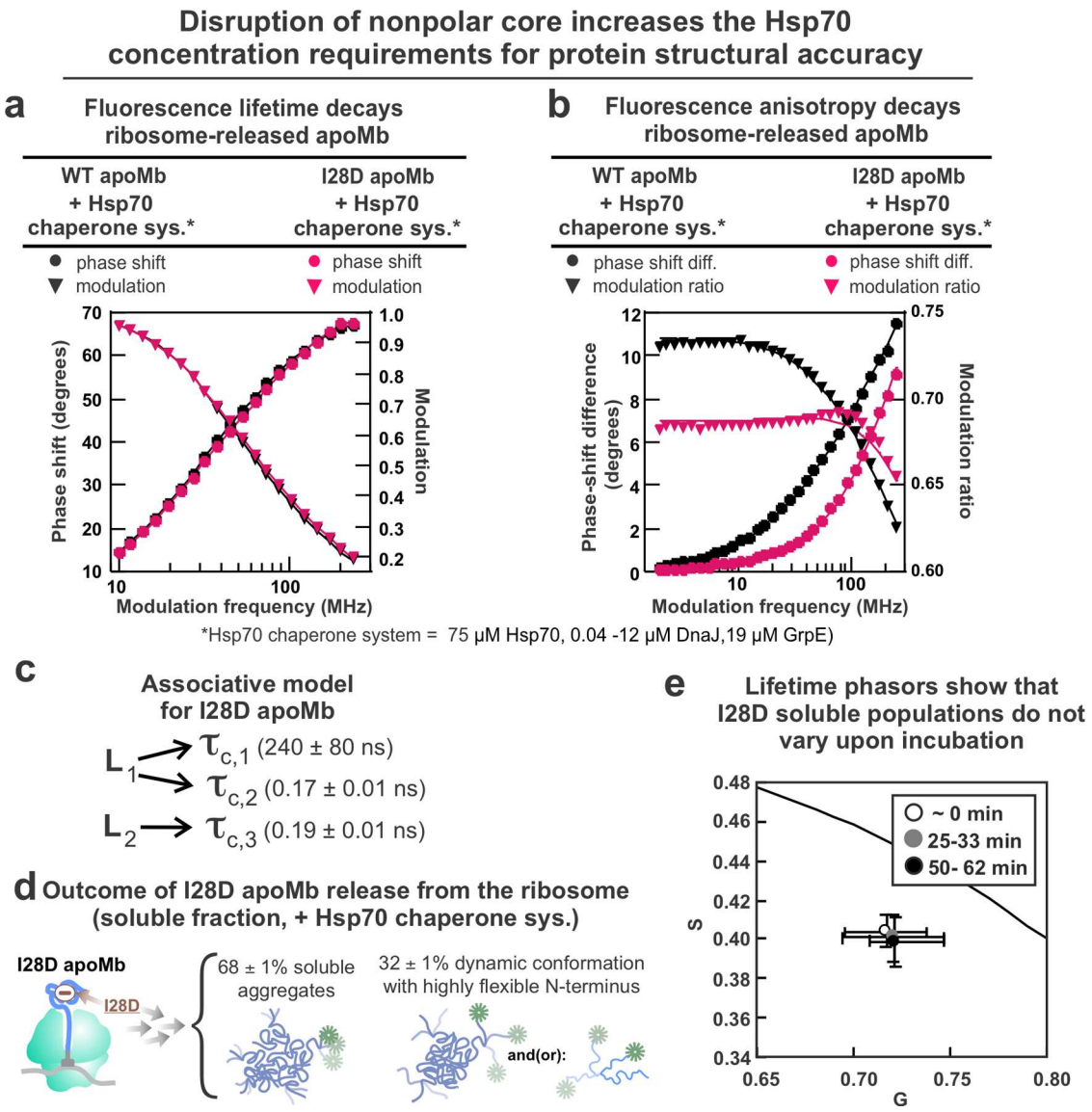


**Figure 10.** Different protein sequences have different Hsp70 chaperone concentration requirements for structural accuracy. (a) Frequency-domain fluorescence lifetime decays of WT apoMb (black) and I28D apoMb (pink) produced in the WT cell-free system in the presence of 75 $\mu$M Hsp70. WT apoMb data is the same data shown in Figure 8a. (b) Frequency-domain fluorescence anisotropy decays of WT apoMb (black) and I28D apoMb (pink) produced in the presence of 75 $\mu$M Hsp70. WT apoMb data is the same data shown in Figure 6d. (c) Simplified representation of associative model used to fit I28D anisotropy data in (d). (d) Cartoon illustrations of I28D apoMb made in the presence of 75 $\mu$M Hsp70. The I28D data fits best to an associative model where there are two detectable populations of species in solution. One population has a large $\tau_c$ value, suggesting the sample contains soluble aggregates. The global $\tau_c$ of the other population cannot be resolved. It has an isotropic fast local motion. (e) Fluorescence lifetime phasors for I28D apoMb made in the presence of 75 $\mu$M Hsp70 and incubated for 1 h after protein synthesis.

observations for WT apoMb. While WT apoMb does not need Hsp70 to prevent the formation of insoluble aggregates at 0.2 $\mu$M apoMb, it needs ca. 300−400 $\mu$M Hsp70 to prevent the formation of soluble aggregates (Figure 8c,d). WT and I28D apoMb have distinct requirement for Hsp70-mediated prevention of soluble-aggregate formation. Further, in the case of I28D apoMb, we were unable to identify any native state formation, upon release from the ribosome. In essence, physiologically relevant concentrations of the Hsp70 chaperone system are insufficient to prevent soluble aggregation of the I28D variant.

In summary, proteins that are soluble are not necessarily well folded. Surprisingly, higher concentrations of Hsp70 are required to prevent soluble aggregate formation compared to insoluble aggregation, indicating that the Hsp70 concentration requirement for structural accuracy is distinct from the concentration requirement for solubility. Further, different protein sequences have different chaperone requirements for solubility and structural accuracy. For some protein variants, physiologically relevant chaperone concentrations may be insufficient to prevent aggregation.

**Release of Newly Synthesized Proteins from the Ribosome Generates Classes of Conformations That Are Kinetically Trapped Relative to Each Other.** The data discussed so far illustrate the fact that ribosome release of de novo synthesized proteins generates two or three distinct classes of conformations. Importantly, all of these conformations are kinetically trapped relative to each other. This concept, which is pictorially illustrated in the cartoons in Figure 11, is justified by the following arguments.


https://doi.org/10.1021/acs.jpcb.2c08485
J. Phys. Chem. B XXXX, XXX, XXX−XXX

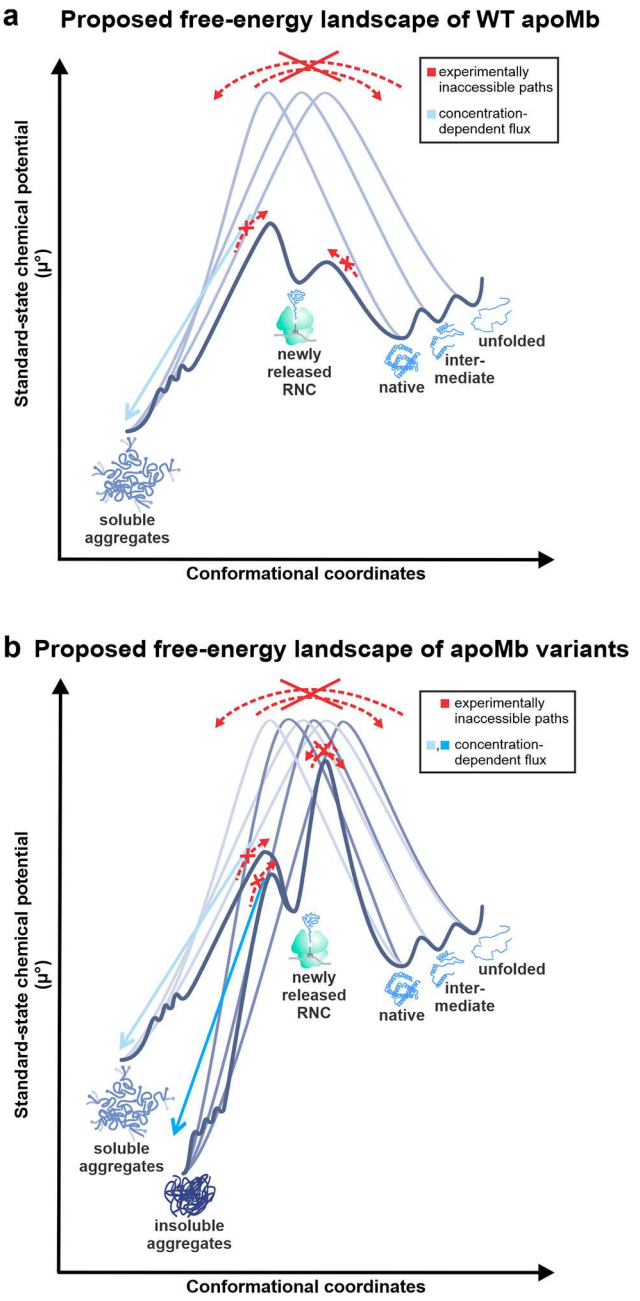


**Figure 11.** Standard-state chemical potential energy landscapes of WT and mutated apoMb. Energy landscapes for (a) WT apoMb and (b) apoMb variants at protein concentration lower (left) and higher (right) than the critical protein concentration for insoluble aggregate formation. Single-point mutations in the apoMb variants increase the kinetic energy barrier between the ribosome-released conformation and the native state.

Data in Figures 6−8 show that, upon release of the ribosome, WT apoMb gives rise to a combination of soluble aggregates and native state. The latter is typically in reversible exchange with intermediates and unfolded states.[48a] Now, lifetime phasors of WT apoMb[3] (Figure 8c) demonstrate that the native state is kinetically trapped from soluble aggregates. Two results provide evidence for this kinetic trapping. First, apoMb generated in the presence of different chaperone concentrations gives rise to phasor points that are located at different positions along a straight line (Figure 8c). Therefore, these samples contain different concentrations of the native state and soluble aggregates. If the two species (i.e., native state and soluble aggregates) were in thermodynamic equilibrium with each other, their relative populations would remain the same regardless of chaperone concentration. Therefore, native state and soluble aggregates must be kinetically trapped relative to each other, and chaperones are somehow able to modulate their relative concentrations in solution. Second, the phasor points do not shift upon 1 h incubation,[3] demonstrating that the kinetic trapping applies to timescale at least as long as this incubation time.

Note that, if native state and soluble aggregates were in equilibrium relative to each other yet below the critical concentration[68] for soluble aggregate formation according to a nucleated polymerization model,[67] time-dependent variations in phasor plots would not be observed. However, the fact that soluble aggregates are present in the system demonstrates that the protein concentration must be above the critical concentration for a phase equilibrium between native-state and soluble aggregate. Yet, this hypothetical equilibrium is inconsistent with the phasor plot results of Figure 8c, as discussed above. In summary, the above arguments show that the native state and soluble aggregates are kinetically trapped relative to each other over a timescale longer than typical *E. coli*'s doubling time (ca. 20−30 min). Further, native state and soluble aggregates must be formed according to parallel paths due to the following reasoning. If the two species were formed sequentially (i.e., from native state to soluble aggregate), given the established kinetic trapping, soluble aggregates would never form. This outcome is in contrast with the experimental evidence for soluble aggregates shown in this work. The cartoon in Figure 11a pictorially recapitulates the above concepts.

The above kinetic trapping between native state and soluble aggregates is detected shortly after translation. Hence, the early stages of protein life assume an utmost importance for WT apoMb, in that they route the newly synthesized protein toward a region of the free-energy landscape that either supports (in the case of native, intermediates and unfolded states) or does not support (in the case of soluble aggregates) biological activity. Therefore, co- and immediately post-translational events effectively determine the entire fate of proteins that, like apoMb, give rise to aggregated species upon release from the ribosome. Further, the role of helpers like the Hsp70 chaperone system is of utmost importance, given that chaperones modulate the relative ratios of native-state and soluble-aggregate components via transient co- and immediately post-translational interactions with newly synthesized proteins. Once released from the ribosome and transient interactions with molecular chaperones are complete, native protein fractions can be biologically active, presumably with no harm from soluble aggregates, which remain kinetically trapped relative to the native state. Soluble aggregates, however, decrease the yield of native state and are often harmful or toxic to cells.[21,22] Therefore, they are generally undesirable.

Kinetic trapping of newly synthesized native states and soluble and insoluble aggregates relative to each other is also applicable to newly synthesized I28D and M131D variants of apoMb. Kinetic trapping of insoluble aggregates relative to the soluble fraction is proven in Figure 5. Parallel paths for the formation of soluble and insoluble fractions of M131D apoMb are proven by published kinetic data from Addabbo et al.[3]


https://doi.org/10.1021/acs.jpcb.2c08485
J. Phys. Chem. B XXXX, XXX, XXX−XXX

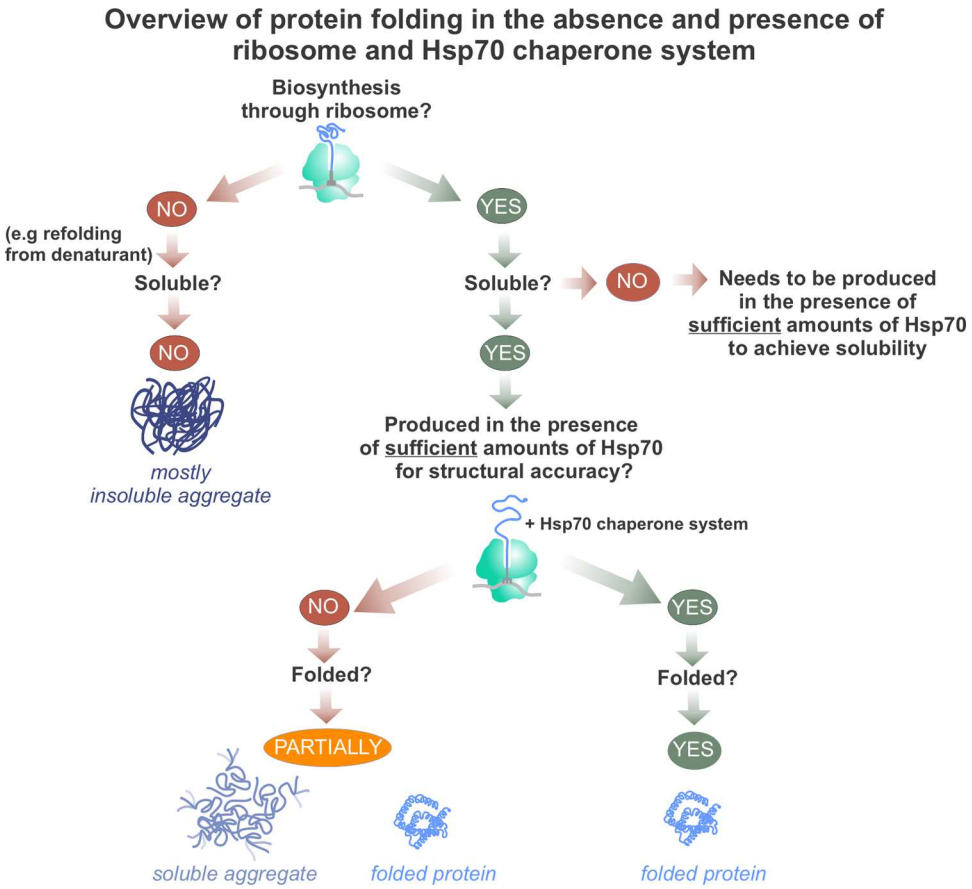


**Figure 12.** Flowchart summarizing the key parameters affecting the generation of soluble and folded proteins in the cellular environment. If a protein has not been biosynthesized through the ribosome, it refolds mainly into an insoluble aggregate, with only very small amounts of soluble folded species. If the protein is biosynthesized through the ribosome in the absence of sufficient Hsp70, it is soluble but not structurally accurate. Only when a protein is synthesized by the ribosome in the presence of sufficient Hsp70, is it both soluble and well folded.

Kinetic trapping of soluble aggregates relative to the native state is consistent with Figure 10e for the I28D apoMb variant and with the above-discussed data for WT apoMb. The cartoon in Figure 11b illustrates the resulting scenario. Namely, newly synthesized native states, soluble aggregates, and insoluble aggregates of the two apoMb variants, which are all experimentally observed (Figures 4−7 and 10, and Addabbo et al.[3]), are trapped relative to each other.

In summary, release from the ribosome can generate undesirable soluble and insoluble aggregates of newly synthesized proteins, in addition to the native state. These three classes of species are kinetically trapped relative to each other, in the case of apoMb and its variant model systems. Therefore, it is crucially important to avoid the formation of soluble and insoluble aggregates at the outset. The correctly folded species generated upon release from the ribosome were indeed shown to persist over long timescales. This scenario may of course be subject to change, but only in case covalent damage or changes in environmental conditions were to modify the free-energy landscape and perturb the extent of kinetic trapping.

We also showed that if the concentrations and client-protein amino acid sequences are sufficiently high and within physiologically relevant ranges, the Hsp70 and TF molecular chaperones contribute to reduce the extent of aggregation upon release from the ribosome. This is unfortunately not always the case, as seen for instance in Figure 8c,d.

Finally, it is worth noting that in vivo overexpression of WT apoMb takes place at concentrations much higher than the cell-free concentrations analyzed in this work. Under these conditions, mostly insoluble aggregates known as inclusion bodies are routinely formed.[26,52] Therefore, upon in vivo overexpression of WT apoMb, a free-energy landscape similar to the one shown here for the variants (Figure 11b) likely also applies to the WT protein.

**Biological Implications.** Our studies highlight the importance of soluble aggregate formation upon release of nascent protein chains from the ribosome. In contrast, prior investigations analyzing protein expression in the absence and presence of chaperones focused primarily on the native state alone or on insoluble aggregates.[6,18]

Further, the data in this work indicate the need to examine client-protein dependence on Hsp70 in a quantitative manner. Different proteins have different Hsp70 concentration needs depending on their sequence and likely other physical properties. In biological research, there is a significant need to be able to produce large quantities of soluble folded protein by overexpression. The co-overexpression of molecular chaperones during protein overexpression in bacteria has shown variable success, to date.

The flowchart in Figure 12 highlights the key parameters that influence the generation of soluble native state, soluble aggregates, and insoluble aggregates within the *E. coli* cellular environment. Our work shows that at sufficient concentrations,


https://doi.org/10.1021/acs.jpcb.2c08485
J. Phys. Chem. B XXXX, XXX, XXX−XXX

chaperones can play a protective role and prevent aggregation caused by mutations. However, physiological concentrations of chaperones are sometimes insufficient to prevent aggregation of some protein variants.

In addition, as highlighted in Figure 13, apoMb variants require higher chaperone concentrations to prevent soluble and insoluble aggregate formation, relative to the wild-type protein. Our findings show that, depending on the specific protein sequence, molecular chaperones at higher concentrations than physiologically attainable may be necessary to generate 100% native states upon protein expression. This observed sequence dependence of chaperone requirements is likely a consequence of the sequence dependence of the relative rates of protein folding and aggregation upon release from the ribosome, as previously shown in the case of WT and M131D apoMb.[3]

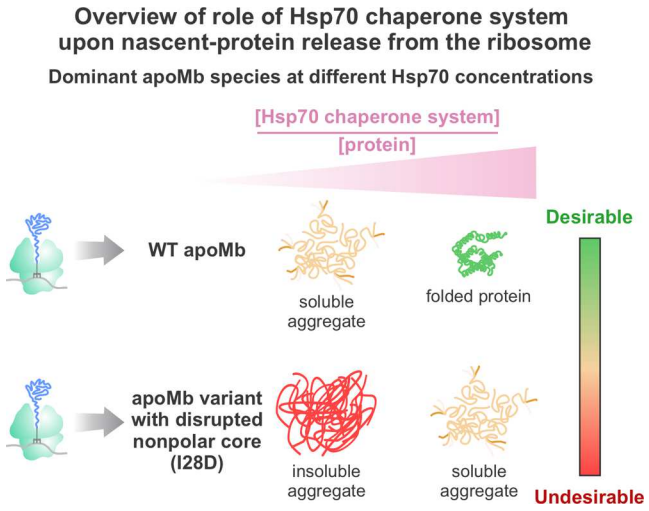


**Figure 13.** Client protein requirements for Hsp70 chaperone system concentration. The Hsp70 concentration requirement for protein structural accuracy is greater than the concentration requirement for protein solubility. The Hsp70 concentration requirements for solubility and structural accuracy depend on the protein sequence. Single-point mutations increase the Hsp70 concentration requirement for protein solubility (I28D and M131D) and structural accuracy (I28D).

Previous work in mammalian cell, yeast, and mouse model systems indicated that heterologous expression of molecular chaperones and upregulation of chaperones by chemical induction of the heat shock response reduce protein aggregation.[78] However, more investigations are necessary to identify whether the necessary chaperone concentrations can in practice always be achieved for the complete prevention of soluble and insoluble aggregate formation upon release from the ribosome.

## CONCLUSIONS

In summary, this work highlights an important role of the bacterial Hsp70 chaperone system during de novo protein biogenesis. Namely, increasing Hsp70 concentration not only decreases the fraction of insoluble translation product (whenever relevant) but also increases the structural accuracy of the soluble gene product by augmenting the fraction of protein native state over soluble aggregates. Small changes in amino-acid sequence (single-point mutations) can dramatically perturb the solubility of nascent proteins upon release from the ribosome. Hsp70 is able to restore this solubility. On the other hand, the concentration of Hsp70 that is sufficient to prevent wild-type and variant client proteins from forming insoluble aggregates is insufficient to prevent soluble-aggregate formation. In essence, Hsp70 concentration requirements for solubility and structural accuracy within the soluble state are distinct, with structural accuracy requiring higher levels of Hsp70 than mere solubility. In the case of the M131D and I28D apoMb variants, the concentration of Hsp70 chaperone system required to generate a fully native client protein upon release from the ribosome exceeds chaperone solubility. This finding suggests that the evolution of other chaperone systems may have arisen to overcome the imperfect nature of the inherent limitations of the Hsp70 chaperone system.

## ASSOCIATED CONTENT

### Supporting Information

The Supporting Information is available free of charge at https://pubs.acs.org/doi/10.1021/acs.jpcb.2c08485.

Evidence for kinetic trapping of soluble and insoluble states; signal-to-noise ratios of NMR resonances used to estimate native-protein concentrations in cell-free systems; additional experiments aiming at further characterization of soluble aggregates; estimation of the concentration of TF; concentration of apoMb in cell-free system; reprocessing anisotropy data reported in Ziehr et al.; experimental volume of apoMb samples; statistical $p$ values for solubility assays; statistical $p$ values for rotational correlation times; statistical $p$ values for lifetimes; fluorescence emission spectra for BODIPY-FL-labeled WT apoMb; and phasor plot of apoMb made in the presence of Hsp70 + Hsp70 inhib. added post-translationally (PDF)

## AUTHOR INFORMATION

### Corresponding Author

**Silvia Cavagnero** − *Biophysics Graduate Degree Program, University of Wisconsin—Madison, Madison, Wisconsin 53706, United States; Department of Chemistry, University of Wisconsin, Madison, Wisconsin 53706, United States;* orcid.org/0000-0002-4290-2331; Phone: 608-262-5430; Email: cavagnero@chem.wisc.edu

### Authors

**Rayna M. Addabbo** − *Biophysics Graduate Degree Program, University of Wisconsin—Madison, Madison, Wisconsin 53706, United States;* Present Address: Institute for Molecular Virology, University of Minnesota-Twin Cities, 18-242 Moos Tower, 515 Delaware St SE, Minneapolis, Minnesota 55455, United States

**Rachel B. Hutchinson** − *Department of Chemistry, University of Wisconsin, Madison, Wisconsin 53706, United States;* orcid.org/0000-0002-9645-2970

**Heather J. Allaman** − *Department of Chemistry, University of Wisconsin, Madison, Wisconsin 53706, United States*

**Matthew D. Dalphin** − *Biophysics Graduate Degree Program, University of Wisconsin—Madison, Madison, Wisconsin 53706, United States*

**Miranda F. Mecha** − *Biophysics Graduate Degree Program, University of Wisconsin—Madison, Madison, Wisconsin 53706, United States*



https://doi.org/10.1021/acs.jpcb.2c08485
J. Phys. Chem. B XXXX, XXX, XXX−XXX

**Yue Liu** − *Department of Chemistry, University of Wisconsin, Madison, Wisconsin 53706, United States*
**Alexios Staikos** − *Department of Chemistry, University of Wisconsin, Madison, Wisconsin 53706, United States;* Present Address: Dana-Farber Cancer Institute, 450 Brookline Avenue, Boston, Massachusetts 02215, United States.

Complete contact information is available at: https://pubs.acs.org/10.1021/acs.jpcb.2c08485

### Notes

The authors declare no competing financial interest.

## ■ ACKNOWLEDGMENTS

The authors thank the National Science Foundation (NSF) for funding (grants MCB-2124672 and CBET 1912259 to S.C.). R.M.A. was the recipient of a National Science Foundation Graduate Research Fellowship Program (grant no. DGE-1256259). Support for this research was also provided by the Graduate School and by the Office of the Vice Chancellor for Research and Graduate Education at the University of Wisconsin-Madison with funding from the Dorothy Powelson Scholarship Fund. R.H. thanks the National Institute of General Medical Sciences of the National Institutes of Health for a TEAM-Science Fellowship (award number R25GM083252). The authors are also grateful to Prof. David Jameson for sharing useful insights and to Justin Dang for helpful discussions. They thank Aaron Hoskins for allowing them to use the Refeyn Two$^{MP}$ instrument and Ye Liu and Brenda Watt for helping them with data collection and analysis with this instrument.

## ■ ABBREVIATIONS

apoMb, apomyoglobin; TF, TF; K/J/E, DnaK/DnaJ/GrpE; RNC, ribosome-bound nascent chain

## ■ REFERENCES

(1) Dalphin, M. D.; Stangl, A. J.; Liu, Y.; Cavagnero, S. KLR-70: A novel cationic inhibitor of the bacterial Hsp70 chaperone. *Biochemistry* **2020**, *59*, 1946−1960.
(2) Kuriyan, J.; Wilz, S.; Karplus, M.; Petsko, G. A. X-ray structure and refinement of carbon-monoxy (Fe II)-myoglobin at 1.5 Å resolution. *J. Mol. Biol.* **1986**, *192*, 133−154.
(3) Addabbo, R. M.; Dalphin, M. D.; Mecha, M. F.; Liu, Y.; Staikos, A.; Guzman-Luna, V.; Cavagnero, S. Complementary role of co- and post-translational events in de novo protein biogenesis. *J. Phys. Chem. B* **2020**, *124*, 6488−6507.
(4) Bakke, C. K.; Jungbauer, L. M.; Cavagnero, S. In vitro expression and characterization of native apomyoglobin under low molecular crowding conditions. *Protein Expr. Purif.* **2006**, *45*, 381−392.
(5) (a) Varela, A. E.; England, K. A.; Cavagnero, S. Kinetic trapping in protein folding. *Protein Eng., Des. Sel.* **2019**, *32*, 103−108. (b) Varela, A. E.; Lang, J. F.; Wu, Y. F.; Dalphin, M. D.; Stangl, A. J.; Okuno, Y.; Cavagnero, S. Kinetic Trapping of Folded Proteins Relative to Aggregates under Physiologically Relevant Conditions. *J. Phys. Chem. B* **2018**, *122*, 7682−7698.
(6) Niwa, T.; Ying, B. W.; Saito, K.; Jin, W.; Takada, S.; Ueda, T.; Taguchi, H. Bimodal protein solubility distribution revealed by an aggregation analysis of the entire ensemble of Escherichia coli proteins. *Proc. Natl. Acad. Sci. U.S.A.* **2009**, *106*, 4201−4206.
(7) Ozawa, K.; Headlam, M. J.; Schaeffer, P. M.; Henderson, B. R.; Dixon, N. E.; Otting, G. Optimization of an Escherichia coli system for cell-free synthesis of selectively N-labelled proteins for rapid analysis by NMR spectroscopy. *Eur. J. Biochem.* **2004**, *271*, 4084−93.
(8) (a) Carra, S.; Alberti, S.; Benesch, J. L. P.; Boelens, W.; Buchner, J.; Carver, J. A.; Cecconi, C.; Ecroyd, H.; Gusev, N.; Hightower, L. E.; Klevit, R. E.; Lee, H. O.; Liberek, K.; Lockwood, B.; Poletti, A.; Timmerman, V.; Toth, M. E.; Vierling, E.; Wu, T. C.; Tanguay, R. M. Small heat shock proteins: multifaceted proteins with important implications for life. *Cell Stress Chaperones* **2019**, *24*, 295−308. (b) Dahiya, V.; Buchner, J.Functional Principles and Regulation of Molecular Chaperones. In *Advances in Protein Chemistry and Structural Biology*; Donev, R., Ed.; Elsevier, 2019; Vol. *114*, pp 1−60. (c) Kim, Y. E.; Hipp, M. S.; Bracher, A.; Hayer-Hartl, M.; Ulrich Hartl, F. Molecular chaperone functions in protein folding and proteostasis. *Annu. Rev. Biochem.* **2013**, *82*, 323−355. (d) Rosenzweig, R.; Nillegoda, N. B.; Mayer, M. P.; Bukau, B. The Hsp70 chaperone network. *Nat. Rev. Mol. Cell Biol.* **2019**, *20*, 665−680.
(9) (a) Deuerling, E.; Schulze-Specking, A.; Tomoyasu, T.; Mogk, A.; Bukau, B. Trigger Factor and DnaK Cooperate in Folding Newly Synthesized Proteins. *Nature* **1999**, *400*, 693−696. (b) Koubek, J.; Schmitt, J.; Galmozzi, C. V.; Kramer, G. Mechanisms of cotranslational protein maturation in bacteria. *Front. Mol. Biosci.* **2021**, *8*, No. 689755.
(10) Eliezer, D.; Wright, P. E. Is apomyoglobin a molten globule? Structural characterization by NMR. *J. Mol. Biol.* **1996**, *263*, 531−8.
(11) Sekhar, A.; Lam, H. N.; Cavagnero, S. Protein folding rates and thermodynamic stability are key determinants for interaction with the Hsp70 chaperone system. *Protein Sci.* **2012**, *21*, 1489−1502.
(12) Chen, X.; Hutchinson, R. B.; Cavagnero, S. Distribution and solvent exposure of Hsp70 chaperone binding sites across the Escherichia coli proteome. *Proteins: Struct., Funct., Bioinf.* **2023**, *91*, 665−678.
(13) (a) Teter, S. A.; Houry, W. A.; Ang, D.; Tradler, T.; Rockabrand, D.; Fischer, G.; Blum, P.; Georgopoulos, C.; Hartl, F. U. Polypeptide flux through bacterial Hsp70: DnaK cooperates with trigger factor in chaperoning nascent chains. *Cell* **1999**, *97*, 755−765. (b) Genevaux, P.; Keppel, F.; Schwager, F.; Langendijk-Genevaux, P. S.; Hartl, F. U.; Georgopoulos, C. In vivo analysis of the overlapping functions of DnaK and trigger factor. *EMBO Rep.* **2004**, *5*, 195−200.
(14) (a) Tripathi, A.; Gupta, K.; Khare, S.; Jain, P. C.; Patel, S.; Kumar, P.; Pulianmackal, A. J.; Aghera, N.; Varadarajan, R. Molecular Determinants of Mutant Phenotypes, Inferred from Saturation Mutagenesis Data. *Mol. Biol. Evol.* **2016**, *33*, 2960−2975. (b) Tripathi, A.; Swaroop, S.; Varadarajan, R. Molecular Determinants of Temperature-Sensitive Phenotypes. *Biochemistry* **2019**, *58*, 1738−1750.
(15) Aguilar-Rodríguez, J.; Sabater-Muñoz, B.; Montagud-Martínez, R.; Berlanga, V.; Alvarez-Ponce, D.; Wagner, A.; Fares, M. A. The molecular chaperone DnaK is a source of mutational robustness. *Genome Biol. Evol.* **2016**, *8*, 2979−2991.
(16) Calloni, G.; Chen, T.; Schermann, S. M.; Chang, H.-c.; Genevaux, P.; Agostini, F.; Tartaglia, G. G.; Hayer-Hartl, M.; Hartl, F. U. DnaK Functions as a Central Hub in the E. coli Chaperone Network. *Cell Rep.* **2012**, *1*, 251−264.
(17) Kadibalban, A. S.; Bogumil, D.; Landan, G.; Dagan, T. DnaK-Dependent Accelerated Evolutionary Rate in Prokaryotes. *Genome Biol. Evol.* **2016**, *8*, 1590−1599.
(18) Niwa, T.; Kanamori, T.; Ueda, T.; Taguchi, H. Global analysis of chaperone effects using a reconstituted cell-free translation system. *Proc. Natl. Acad. Sci. U.S.A.* **2012**, *109*, 8937.
(19) Fatima, K.; Naqvi, F.; Younas, H. A Review: Molecular Chaperone-mediated Folding, Unfolding and Disaggregation of Expressed Recombinant Proteins. *Cell Biochem. Biophys.* **2021**, *79*, 153−174.
(20) de Marco, A.; Laszlo, V.; Sophia, D.; Pierre, G. Native folding of aggregation-prone recombinant proteins in Escherichia coli by osmolytes, plasmid- or benzyl alcohol−overexpressed molecular chaperones. *Cell Stress Chaperones* **2005**, *10*, 329−339.
(21) Haacke, A.; Fendrich, G.; Ramage, P.; Geiser, M. Chaperone over-expression in Escherichia coli: Apparent increased yields of soluble recombinant protein kinases are due mainly to soluble aggregates. *Protein Expr. Purif.* **2009**, *64*, 185−193.

(22) (a) Cascella, R.; Bigi, A.; Cremades, N.; Cecchi, C. Effects of oligomer toxicity, fibril toxicity and fibril spreading in synucleinopathies. *Cell. Mol. Life Sci.* **2022**, *79*, No. 174. (b) Cline, E. N.; Bicca, M. A.; Viola, K. L.; Klein, W. L. The Amyloid-$\beta$ Oligomer Hypothesis: Beginning of the Third Decade. *J. Alzheimers Dis.* **2018**, *64*, S567−S610. (c) Mallucci, G. R.; Klenerman, D.; Rubinsztein, D. C. Developing therapies for neurodegenerative disorders: Insights from protein aggregation and cellular stress responses. *Annu. Rev. Cell Dev. Biol.* **2020**, *36*, 165−189.

(23) (a) Breslow, E.; Beychok, S.; Hardman, K. D.; Gurd, F. R. N. Relative Conformations of Sperm Whale Metmyoglobin and Apomyoglobin in Solution. *J. Biol. Chem.* **1965**, *240*, 304. (b) Cavagnero, S.; Nishimura, C.; Schwarzinger, S.; Dyson, H. J.; Wright, P. E. Conformation and dynamic characterization of the molten globule state of an apomyoglobin mutant with an altered folding pathway. *Biochemistry* **2001**, *40*, 14459−14467. (c) Cavagnero, S.; Dyson, H. J.; Wright, P. E. Effect of H helix destabilizing mutations on the kinetic and equilibrium folding of apomyoglobin. *J. Mol. Biol.* **1999**, *285*, 269−282. (d) Eliezer, D.; Jennings, P. A.; Dyson, H. J.; Wright, P. E. Populating the equilibrium molten globule state of apomyoglobin under conditions suitable for structural characterization by NMR. *FEBS Lett.* **1997**, *417*, 92−96. (e) Jungbauer, L. M.; Bakke, C. K.; Cavagnero, S. Experimental and computational analysis of translation products in apomyoglobin expression. *J. Mol. Biol.* **2006**, *357*, 1121−1143. (f) Postnikova, G. B.; Yumakova, E. M. Fluorescence Study of the Conformational Properties of Myoglobin Structure. 3. pH-Dependent Changes in Porphyrin and Tryptophan Fluorescence o the Complex of Sperm Whale Apomyoglobin with the Protoporphyrin-IX - The Role of the Porphyrin Macrocycle and Iron in Formation of Native Myoglobin Structure. *Eur. J. Biochem.* **1991**, *198*, 241−246. (g) Tsui, V.; Garcia, C.; Cavagnero, S.; Siuzdak, G.; Dyson, H. J.; Wright, P. E. Quench-Flow Experiments Combined with Mass Spectrometry Show Apomyoglobin Folds through an Obligatory Intermediate. *Protein Sci.* **2008**, *8*, 45−49.

(24) Hesterkamp, T.; Bukau, B. Role of the DnaK and HscA homologs of Hsp70 chaperones in protein folding in *E coli*. *EMBO J.* **1998**, *17*, 4818−4828.

(25) Ellis, J. P.; Bakke, C. K.; Kirchdoerfer, R. N.; Jungbauer, L. M.; Cavagnero, S. Chain dynamics of nascent polypeptides emerging from the ribosome. *ACS Chem. Biol.* **2008**, *3*, 555−566.

(26) Chow, C. C.; Chow, C.; Raghunathan, V.; Huppert, T. J.; Kimball, E. B.; Cavagnero, S. Chain length dependence of apomyoglobin folding: structural evolution from misfolded sheets to native helices. *Biochemistry* **2003**, *42*, 7090−9.

(27) (a) Schneider, C. A.; Rasband, W. S.; Eliceiri, K. W. NIH Image to ImageJ: 25 years of image analysis. *Nat. Methos* **2012**, *9*, 671−675. (b) Abràmoff, M. D.; Magalhães, P. J.; Ram, S. J. Image processing with ImageJ. *Biophotonics Int.* **2004**, *11*, 36−42.

(28) Kirchdoerfer, R. N.; Huang, J. J.; Isola, M. K.; Cavagnero, S. Fluorescence-based analysis of aminoacyl- and peptidyl-tRNA by low-pH sodium dodecyl sulfate-polyacrylamide gel electrophoresis. *Anal. Biochem.* **2007**, *364*, 92−4.

(29) (a) Lee, J. H.; Zhang, D. Y.; Hughes, C.; Okuno, Y.; Sekhar, A.; Cavagnero, S. Heterogeneous binding of the SH3 client protein to the DnaK molecular chaperone. *Proc. Natl. Acad. Sci. U.S.A.* **2015**, *112*, E4206−E4215. (b) Sekhar, A.; Santiago, M.; Lam, H. N.; Lee, J. H.; Cavagnero, S. Transient interactions of a slow-folding protein with the Hsp70 chaperone machinery. *Protein Sci.* **2012**, *21*, 1042−1055.

(30) Gill, S. C.; Vonhippel, P. H. Calculation of protein extinction coefficients from amino acid sequence data. *Anal. Biochem.* **1989**, *182*, 319−326.

(31) Guzman-Luna, V.; Fuchs, A. M.; Allen, A. J.; Staikos, A.; Cavagnero, S. An intrinsically disordered nascent protein interacts with specific regions of the ribosomal surface near the exit tunnel. *Commun. Biol.* **2021**, *4*, No. 1236.

(32) Knight, A. M.; Culviner, P. H.; Kurt-Yilmaz, Ne.; Zou, T.; Ozkan, S. B.; Cavagnero, S. Electrostatic effect of the ribosomal surface on nascent polypeptide dynamics. *ACS Chem. Biol.* **2013**, *8*, 1195−1204.

(33) Ross, J. A.; Jameson, D. M. Time-resolved methods in biophysics. 8. Frequency domain fluorometry: applications to intrinsic protein fluorescence. *Photochem. Photobiol. Sci.* **2008**, *7*, 1301−1312.

(34) Štefl, M.; James, N. G.; Ross, J. A.; Jameson, D. M. Applications of phasors to in vitro time-resolved fluorescence measurements. *Anal. Biochem.* **2011**, *410*, 62−69.

(35) Weinreis, S. A.; Ellis, J. P.; Cavagnero, S. Dynamic fluorescence depolarization: A powerful tool to explore protein folding on the ribosome. *Methods* **2010**, *52*, 57−73.

(36) Ellis, J. P.; Culviner, P. H.; Cavagnero, S. Confined dynamics of a ribosome-bound nascent globin: Cone angle analysis of fluorescence depolarization decays in the presence of two local motions. *Protein Sci.* **2009**, *18*, 2003−2015.

(37) Ziehr, D. R.; Ellis, J. P.; Culviner, P. H.; Cavagnero, S. Production of ribosome-released nascent proteins with optimal physical properties. *Anal. Chem.* **2010**, *82*, 4637−4643.

(38) (a) Kleckner, I. R.; Foster, M. P. An introduction to NMR-based approaches for measuring protein dynamics. *Biochim. Biophys. Acta, Proteins Proteomics* **2011**, *1814*, 942−968. (b) Odin, C. NMR studies of phase transitions. *Annu. Rep. NMR Spect.* **2006**, *59*, 117−205 Webb, G. A., Ed.. (c) Rajagopalan, S.; Kurt, N.; Cavagnero, S. High-Resolution Conformation and Backbone Dynamics of a Soluble Aggregate of Apomyoglobin(119). *Biophys. J.* **2011**, *100*, 747−755.

(39) Rajagopalan, S.; Chow, C.; Raghunathan, V.; Fry, C. G.; Cavagnero, S. NMR spectroscopic filtration of polypeptides and proteins in complex mixtures. *J. Biomol. NMR* **2004**, *29*, 505−516.

(40) Ernst, R. R.; Bodenhausen, G.; Wokaun, A., *Principles of Nuclear Magnetic Resonance in One and Two Dimensions*; Oxford University Press: New York, 1989.

(41) Rüdiger, S.; Germeroth, L.; Schneider-Mergener, J.; Bukau, B. Substrate specificity of the DnaK chaperone determined by screening cellulose-bound peptide libraries. *EMBO J.* **1997**, *16*, 1501−1507.

(42) (a) Lecomte, J. T. J.; Vuletich, D. A.; Lesk, A. M. Structural divergence and distant relationships in proteins: evolution of the globins. *Curr. Opin. Struct. Biol.* **2005**, *15*, 290−301. (b) Vinogradov, S. N.; Hoogewijs, D.; Bailly, X.; Arredondo-Peter, R.; Gough, J.; Dewilde, S.; Moens, L.; Vanfleteren, J. R. A phylogenomic profile of globins. *BMC Evol. Biol.* **2006**, *6*, No. 31. (c) Wu, G. H.; Wainwright, L. M.; Poole, R. K.Microbial Globins. In *Advances in Microbial Physiology*; Elsevier, 2003; Vol. *47*, pp 255−310.

(43) Lecomte, J. T. J.; Sukits, S. F.; Bhattacharya, S.; Falzone, C. J. Conformational properties of native sperm whale apomyoglobin in solution. *Protein Sci.* **1999**, *8*, 1484−1491.

(44) Hutchinson, R. B.; Chen, X.; Zhou, N. K.; Cavagnero, S. Fluorescence Anisotropy Decays and Microscale-Volume Viscometry Reveal the Compaction of Ribosome-Bound Nascent Proteins. *J. Phys. Chem. B* **2021**, *125*, 6543−6558.

(45) Yaeger-Weiss, S. K.; Jennaro, T. S.; Mecha, M.; Becker, J. H.; Yang, H. M.; Winkler, G. L. W.; Cavagnero, S. Net Charge and Nonpolar Content Guide the Identification of Folded and Prion Proteins. *Biochemistry* **2020**, *59*, 1881−1895.

(46) Springer, B. A.; Sligar, S. G. High-level expression of sperm whale myoglobin in *Escherichia coli*. *Proc. Natl. Acad. Sci. U.S.A.* **1987**, *84*, 8961−8965.

(47) (a) Barrick, D.; Baldwin, R. L. 3-state analysis of sperm whale apomyoglobin folding. *Biochemistry* **1993**, *32*, 3790−3796. (b) Shen, L. L.; Hermans, J. Kinetics of Conformation Change of Sperm-Whale Myoglobin. 3. Folding and Unfolding of Apomyoglobin and Suggested Overall Mechanism. *Biochemistry* **1972**, *11*, 1845−1849.

(48) (a) Dyson, H. J.; Wright, P. E. How does your protein fold? Elucidating the apomyoglobin folding pathway. *Acc. Chem. Res.* **2017**, *50*, 105−111. (b) Garcia, C.; Nishimura, C.; Cavagnero, S.; Dyson, H. J.; Wright, P. E. Changes in the apomyoglobin folding pathway caused by mutation of the distal histidine residue. *Biochemistry* **2000**, *39*, 11227−11237. (c) Jennings, P. A.; Wright, P. E. Formation of a molten globule intermediate early in the kinetic folding pthway of apomyoglobin. *Science* **1993**, *262*, 892−896.

(49) (a) Cavagnero, S.; Kurt, N. Folding and Misfolding as a Function of Polypeptide Chain Elongation: Conformational Trends



https://doi.org/10.1021/acs.jpcb.2c08485
J. Phys. Chem. B XXXX, XXX, XXX−XXX

and Implications for Intracellular Events. In *Misbehaving Proteins: Protein (Mis)Folding, Aggregation and Stability*; Murphy, R.; Tsai, A., Eds.; Kluwer Academic Press, 2006; pp 217−246. (b) Jungbauer, L. M.; Bakke, C.; Cavagnero, S. Experimental and computational analysis of translation products in apomyoglobin expression. *J. Mol. Biol.* **2006**, *357*, 1121−1143. (c) Kurt, N.; Cavagnero, S. Nonnative helical motif in a chaperone-bound protein fragment. *Biophys. J.* **2008**, *94*, L48−L50.

(50) To, P.; Whitehead, B.; Tarbox, H. E.; Fried, S. D. Nonrefoldability is Pervasive Across the E. coli Proteome. *J. Am. Chem. Soc.* **2021**, *143*, 11435−11448.

(51) Chow, C.; Kurt, N.; Murphy, R. M.; Cavagnero, S. Structural characterization of apomyoglobin self-associated species in aqueous buffer and urea solution. *Biophys. J.* **2006**, *90*, 298−309.

(52) Jennings, P. A.; Stone, M. J.; Wright, P. E. Overexpression of myoglobin and assignment of its amide, C-alpha and C-beta resonances. *J. Biomol. NMR* **1995**, *6*, 271−276.

(53) Vega, C. A.; Kurt, N.; Chen, Z.; Rüdiger, S.; Cavagnero, S. Binding specificity of an $\alpha$-helical protein sequence to a full-length Hsp70 chaperone and its minimal substrate-binding domain. *Biochemistry* **2006**, *45*, 13835−13846.

(54) Kurt, N.; Rajagopalan, S.; Cavagnero, S. Effect of Hsp70 Chaperone on the Folding and Misfolding of Polypeptides Modeling an Elongating Protein Chain. *J. Mol. Biol.* **2006**, *355*, 809−820.

(55) Bakke, C. K.; Jungbauer, L. M.; Cavagnero, S. *In vitro* expression and characterization of native apomyoglobin under low molecular crowding conditions. *Prot. Expr. Purif.* **2006**, *45*, 381−392.

(56) Denisov, V. P.; Schlessman, J. L.; Garcia-Moreno, B.; Halle, B. Stabilization of internal charges in a protein: Water penetration or conformational change? *Biophys. J.* **2004**, *87*, 3982−3994.

(57) Spudich, G. M.; Miller, E. J.; Marqusee, S. Destabilization of the Escherichia coli RNase H kinetic intermediate: switching between a two-state and three-state folding mechanism. *J. Mol. Biol.* **2004**, *335*, 609−618.

(58) (a) Wilson, D. N.; Beckmann, R. The ribosomal tunnel as a functional environment for nascent polypeptide folding and translational stalling. *Curr. Opin. Struct. Biol.* **2011**, *21*, 274−82. (b) Schuwirth, B. S.; Borovinskaya, M. A.; Hau, C. W.; Zhang, W.; Vila-Sanjurjo, A.; Holton, J. M.; Cate, J. H. Structures of the bacterial ribosome at 3.5 A resolution. *Science* **2005**, *310*, 827−34. (c) Selmer, M.; Dunham, C. M.; Murphy, F. V.; Weixlbaumer, A.; Petry, S.; Kelley, A. C.; Weir, J. R.; Ramakrishnan, V. Structure of the 70S ribosome complexed with mRNA and tRNA. *Science* **2006**, *313*, 1935−1942.

(59) Voss, N. R.; Gerstein, M.; Steitz, T. A.; Moore, P. B. The geometry of the ribosomal polypeptide exit tunnel. *J. Mol. Biol.* **2006**, *360*, 893−906.

(60) Malkin, L. I.; Rich, A. Partial resistance of nascent polypeptide chains to proteolytic digestion due to ribosomal shielding. *J. Mol. Biol.* **1967**, *26*, 329−346.

(61) (a) Guinn, E. J.; Pegram, L. M.; Capp, M. W.; Pollock, M. N.; Record, M. T. Quantifying why urea is a protein denaturant, whereas glycine betaine is a protein stabilizer. *Proc. Natl. Acad. Sci. U.S.A.* **2011**, *108*, 16932−16937. (b) Myers, J. K.; Pace, C. N.; Scholtz, J. M. Denaturant m-values and heat capacity changes - relation to changes in accessble surface areas of protein unfolding. *Protein Sci.* **1995**, *4*, 2138−2148. (c) Scholtz, J. M.; Grimsley, G. R.; Pace, C. N.Solvent denaturation of proteins and interpretation of the m value. In *Methods in Enzymology: Biothermodynamics, Part B*; Johnson, M. L.; Holt, J. M.; Ackers, G. K., Eds.; Elsevier, 2009; Vol. *466*, pp 549−565.

(62) (a) Harms, M. J.; Castaneda, C. A.; Schlessman, J. L.; Sue, G. R.; Isom, D. G.; Cannon, B. R.; Garcia-Moreno, B. The pK(a) Values of Acidic and Basic Residues Buried at the Same Internal Location in a Protein Are Governed by Different Factors. *J. Mol. Biol.* **2009**, *389*, 34−47. (b) Robinson, A. C.; Majumdar, A.; Schlessman, J. L.; Garcia-Moreno, B. Charges in Hydrophobic Environments: A Strategy for Identifying Alternative States in Proteins. *Biochemistry* **2017**, *56*, 212−218.

(63) (a) Hazlett, T. L.; Jameson, D. M. Time-Resolved Laser Spectroscopy in Biochemistry. In *Time-Resolved Fluorescence Studies on Components of the Prokaryotic Protein Elongation system*; International Society for Optics and Photonics, 1988; pp 412−419. (b) Jameson, D. M.; Gratton, E.; Hall, R. D. The measurement and analysis of heterogeneous emissions by multifrequency phase and modulation fluorometry. *Appl. Spectrosc. Rev.* **1984**, *20*, 55−106.

(64) Lakowicz, J. R. *Principles of Fluorescence Spectroscopy*, 3rd ed.; Plenum Press: New York, 2006.

(65) Fedyukina, D. V.; Jennaro, T. S.; Cavagnero, S. Charge Segregation and Low Hydrophobicity Are Key Features of Ribosomal Proteins from Different Organisms. *J. Biol. Chem.* **2014**, *289*, 6740−6750.

(66) (a) Kaiser, C. M.; Chang, H. C.; Agashe, V. R.; Lakshmipathy, S. K.; Etchells, S. A.; Hayer-Hartl, M.; Hartl, F. U.; Barral, J. M. Real-time observation of trigger factor function on translating ribosomes. *Nature* **2006**, *444*, 455−460. (b) Beck, K.; Wu, L. F.; Brunner, J.; Muller, M. Discrimination between SRP- and SecA/SecB-dependent substrates involves selective recognition of nascent chains by SRP and trigger factor. *EMBO J.* **2000**, *19*, 134−143. (c) De Geyter, J.; Portaliou, A. G.; Srinivasu, B.; Krishnamurthy, S.; Economou, A.; Karamanou, S. Trigger factor is a bona fide secretory pathway chaperone that interacts with SecB and the translocase. *EMBO Rep.* **2020**, *21*, No. e49054. (d) Liu, C. P.; Perrett, S.; Zhou, J. M. Dimeric trigger factor stably binds folding-competent intermediates and cooperates with the DnaK-DnaJ-GrpE chaperone system to allow refolding. *J. Biol. Chem.* **2005**, *280*, 13315−13320. (e) Yang, F.; Chen, T. Y.; Krzeminski, L.; Santiago, A. G.; Jung, W.; Chen, P. Single-molecule dynamics of the molecular chaperone trigger factor in living cells. *Mol. Microbiol.* **2016**, *102*, 992−1003.

(67) (a) Oosawa, F.; Kasai, M. A theory of linear and helical aggregations of macromolecules. *J. Mol. Biol.* **1962**, *4*, 10−21. (b) Oosawa, F.; Asakura, S. *Thermodynamics of the Polymerization of Protein*; Academic Press, 1975.

(68) Tanford, C. *The Hydrophobic Effect: Fomation of Micelles and Biological Membranes*; John Wyley & Sons, 1973.

(69) (a) Deyoung, L. R.; Dill, K. A.; Fink, A. L. Aggregation and denaturation of apomyoglobin in aqueous urea solutions. *Biochemistry* **1993**, *32*, 3877−3886. (b) Kar, K.; Jayaraman, M.; Sahoo, B.; Kodali, R.; Wetzel, R. Critical nucleus size for disease-related polyglutamine aggregation is repeat length dependent. *Nat. Struct. Mol. Biol.* **2011**, *18*, 328−336.

(70) (a) Bartolucci, G.; Adame-Arana, O.; Zhao, X. P.; Weber, C. A. Controlling composition of coexisting phases via molecular transitions. *Biophys. J.* **2021**, *120*, 4682−4697. (b) Fritsch, A. W.; Diaz-Delgadillo, A. F.; Adame-Arana, O.; Hoege, C.; Mittasch, M.; Kreysing, M.; Leaver, M.; Hyman, A. A.; Julicher, F.; Weber, C. A. Local thermodynamics govern formation and dissolution of Caenorhabditis elegans P granule condensates. *Proc. Natl. Acad. Sci. U.S.A.* **2021**, *118*, No. e2102772118. (c) Eeftens, J. M.; Kapoor, M.; Michieletto, D.; Brangwynne, C. P. Polycomb condensates can promote epigenetic marks but are not required for sustained chromatin compaction. *Nat. Commun.* **2021**, *12*, No. 5888. (d) Zeigler, T. M.; Chung, M. C.; Narayan, O. P.; Guan, J. Protein phase separation: physical models and phase-separation- mediated cancer signaling. *Adv. Phys. X* **2021**, *6*, No. 1936638. (e) Peran, I.; Martin, E. W.; Mittag, T.Walking Along a Protein Phase Diagram to Determine Coexistence Points by Static Light Scattering. In *Intrinsically Disordered Proteins: Methods and Protocols*; Kragelund, B. B.; Skriver, K., Eds.; Springer, 2020; Vol. *2141*, pp 715−730.

(71) Jameson, D. M. *Introduction to Fluorescence*; CRC Press, 2014.

(72) Lakowicz, J. R.; Cherek, H.; Laczko, G.; Gratton, E. Time-resolved fluorescence emission-spectra of labeled phospholipid vesicles as observed using multi-frequency phase modulation fluorometry. *Biochim. Biophys. Acta, Biomembr.* **1984**, *777*, 183−193.

(73) (a) Bosson, J.; Gouin, J.; Lacour, J. Cationic triangulenes and helicenes: synthesis, chemical stability, optical properties and extended applications of these unusual dyes. *Chem. Soc. Rev.* **2014**, *43*, 2824−2840. (b) Maliwal, B. P.; Fudala, R.; Raut, S.; Kokate, R.;



https://doi.org/10.1021/acs.jpcb.2c08485
J. Phys. Chem. B XXXX, XXX, XXX−XXX

Sørensen, T. J.; Laursen, B. W.; Gryczynski, Z.; Gryczynski, I. Long-lived bright red emitting azaoxa-triangulenium fluorophores. *PLoS One* **2013**, *8*, No. e63043.
(74) Bevington, P.; Robinson, D. K. *Data Reduction and Error Analysis for the Physical Sciences*, 3rd ed.; McGraw Hill Education, 2002.
(75) James, N. G.; Ross, J. A.; Štefl, M.; Jameson, D. M. Applications of phasor plots to in vitro protein studies. *Anal. Biochem.* **2011**, *410*, 70−76.
(76) (a) Komar, A. A.; Kommer, A.; Krasheninnikov, I. A.; Spirin, A. S. Cotranslational heme binding to nascent globin chains. *FEBS Lett.* **1993**, *326*, 261−263. (b) Komar, A. A.; Kommer, A.; Krasheninnikov, I. A.; Spirin, A. S. Cotranslational folding of globin. *J. Biol. Chem.* **1997**, *272*, 10646−10651.
(77) (a) Szmacinski, H.; Jayaweera, R.; Cherek, H.; Lakowicz, J. R. Demonstration of an associated anisotropy decay by frequency-domain fluorometry. *Biophys. Chem.* **1987**, *27*, 233−241. (b) Bialik, C. N.; Wolf, B.; Rachofsky, E. L.; Ross, J. A.; Laws, W. R. Dynamics of biomolecules: assignment of local motions by fluorescence anisotropy decay. *Biophys. J.* **1998**, *75*, 2564−2573.
(78) (a) Klaips, C. L.; Jayaraj, G. G.; Hartl, F. U. Pathways of cellular proteostasis in aging and disease. *J. Cell Biol.* **2018**, *217*, 51−63. (b) Muchowski, P. J.; Schaffar, G.; Sittler, A.; Wanker, E. E.; Hayer-Hartl, M. K.; Hartl, F. U. Hsp70 and Hsp40 chaperones can inhibit self-assembly of polyglutamine proteins into amyloid-like fibrils. *Proc. Natl. Acad. Sci. U.S.A.* **2000**, *97*, 7841−7846. (c) Sittler, A.; Lurz, R.; Lueder, G.; Priller, J.; Hayer-Hartl, M. K.; Hartl, F. U.; Lehrach, H.; Wanker, E. E. Geldanamycin activates a heat shock response and inhibits huntingtin aggregation in a cell culture model of Huntington's disease. *Hum. Mol. Genet.* **2001**, *10*, 1307−1315. (d) Nagy, M.; Fenton, W. A.; Li, D.; Furtak, K.; Horwich, A. L. Extended survival of misfolded G85R SOD1-linked ALS mice by transgenic expression of chaperone Hsp110. *Proc. Natl. Acad. Sci. U.S.A.* **2016**, *113*, 5424−5428. (e) Chaudhury, S.; Keegan, B. M.; Blagg, B. S. J. The role and therapeutic potential of Hsp90, Hsp70, and smaller heat shock proteins in peripheral and central neuropathies. *Med. Res. Rev.* **2021**, *41*, 202−222. (f) Klucken, J.; Shin, Y.; Masliah, E.; Hyman, B. T.; McLean, P. J. Hsp70 reduces alpha-synuclein aggregation and toxicity. *J. Biol. Chem.* **2004**, *279*, 25497−25502. (g) Shen, H. Y.; He, J. C.; Wang, Y. M.; Huang, Q. Y.; Chen, J. F. Geldanamycin induces heat shock protein 70 and protects against MPTP-induced dopaminergic neurotoxicity in mice. *J. Biol. Chem.* **2005**, *280*, 39962−39969. (h) Flower, T. R.; Chesnokova, L. S.; Froelich, C. A.; Dixon, C.; Witt, S. N. Heat shock prevents alpha-synuclein-induced apoptosis in a yeast model of Parkinson's disease. *J. Mol. Biol.* **2005**, *351*, 1081−1100.


https://doi.org/10.1021/acs.jpcb.2c08485
J. Phys. Chem. B XXXX, XXX, XXX−XXX